# 32. EFFECTS OF ATMOSPHERIC REFRACTION ON FAR-FIELD SOUND PROPAGATION

By Orvel E. Smith

NASA George C. Marshall Space Flight Center

32

## SUMMARY

Far-field sound intensity levels are calculated by using a theoretical model based on refraction laws. The theoretical model requires a knowledge of the sound-source characteristics and the velocity-of-sound profile. The velocity-of-sound profile is derived from virtual temperature, wind speed, and wind direction, which are either measured or predicted. The necessary simplifying assumptions used in deriving the theoretical model are discussed. The sound intensity level as derived from the theoretical model and empirical measurements from static firings of the Saturn booster are compared. Practical operation techniques used in obtaining atmospheric measurements, atmospheric predictions, and sound-intensity-level calculations for the static firing of large boosters are discussed.

## INTRODUCTORY DISCUSSION

### Characteristics of Sound Source

In order to indicate the magnitude of the sound generated from several aerospace boosters, a comparison of the estimated total acoustical power level for Jupiter, Saturn I, Saturn V, and a 20-million-pound-thrust booster is presented in figure 1. The values are determined by assuming an exhaust velocity for the engines and by assuming that 1 percent of the jet total power is converted into acoustical power. An increase of only 10 dB for the total acoustical power level of the 1.5-million-pound-thrust engine over that of the 0.15-million-pound-thrust engine is not an impressive increase. However, of greater importance is the fact that as the engine thrust increases, a larger part of the acoustical energy is generated at the lower frequencies. The theoretically derived power levels do not form an estimate of the frequency dependence of the acoustical energy. For this reason experimental values for the acoustical power level are needed. It is known (ref. 1) that the power spectrum of peak acoustical energy for the Jupiter engine shifts by 1 octave toward the lower frequencies of Saturn I. The acoustical energy generated by the Saturn I engine peaks between 10 cps and 100 cps (ref. 1). The lower the frequency, the smaller the acoustical attenuation is for sound propagation through the atmosphere, and thus the greater the possibility is of disturbances to the surrounding communities. Also, the lower the frequencies, the higher the probability becomes that building

structures will be damaged as a result of acoustical energy resonating with the natural frequencies of building structures. The sound directivity of the source is also an important characteristic of the sound source. The study of sound propagation can be approached from three interrelated uisciplines: (1) the characteristic of the sound source; (2) the propagating media; and (3) the response of the receiver.

## Inverse Square Law for Sound Propagation

By using the estimated total acoustical power level for the Jupiter, Saturn I, and Saturn V vehicles and the assumptions of the inverse square law for sound propagation, the overall sound pressure level in decibels (dB re: $10^{-13}$ watt) as a function of distance from the sound source is calculated (see fig. 2). The value of 110 dB has been selected as a critical overall sound pressure level in terms of disturbances to the surrounding community. The radius for the critical sound pressure level, with the assumption of the inverse square law, is 10 km for the Saturn I and 19 km for the Saturn V. Under the assumption of the inverse square law for sound propagation, the prediction would be that every time a Saturn V is static fired at George C. Marshall Space Flight Center (MSFC), an overall sound pressure level equal to or greater than 110 dB would result over the city of Huntsville, Alabama, as well as over a number of surrounding communities (a populated area of approximately 200 000 inhabitants). (See fig. 3.)

The inverse square law assumes a homogeneous medium through which the acoustical energy is propagated; that is, the velocity of sound with respect to altitude and horizontal distance is constant. Although this condition never exists in the real atmosphere, the inverse square law has some theoretical value in understanding certain boundary or limiting conditions for the propagation of sound through the atmosphere and gives a first estimate of the magnitude of the problem for far-field sound intensity levels.

## Approaches to Problem of Far-Field Acoustics

In view of the overall sound pressure level as a function of distance from the sound source as estimated by the inverse square law, the question of what can be done to reduce the problem of sound generated by the large engines arises. Three approaches are followed:

(1) Locating the sound source in a remote area (A new static test facility located in a less densely populated area has been developed; the MSFC-Mississippi Test Facility (MTF) located in southern Mississippi has been in operation since early 1966, Static firings of the Saturn V booster (S-IC) and F-1 engines have continued at MSFC in Huntsville, but on a reduced firing schedule.)

(2) Suppressing the sound at the source (The MSFC Test Laboratory has a working sound-suppression model. From this model, sound-suppression techniques can be studied, and the feasibility of engineering a full-scale sound-suppression system can be determined.)

(3) Restricting the operation (This approach consists of three parts; first, the relationship between atmospheric conditions and sound propagation is determined; then, the atmospheric conditions which cause anomalous sound propagation are predicted; and, finally, static tests are restricted to those conditions which will not produce high sound pressure levels in the surrounding communities. This approach is discussed in detail subsequently.)

## RAY ACOUSTICS AND SOUND INTENSITY LEVEL

One method that has been used by several investigators (refs. 2 to 4) to study the relationship between atmospheric conditions and sound propagation over long distances is known as ray acoustics or sound ray tracing technique. Essentially, the acoustical equivalence to Snell's refraction law is derived and a system of practical equations developed to obtain the ray patterns. By definition, a ray is a curve whose tangent everywhere points in the direction in which the energy contained in the vibrating element is propagated. The derivation of the acoustical equivalence to Snell's refraction law is not presented herein since the derivation in view of the applications to the acoustic problem at MSFC is presented in detail by Heybey in reference 5 and more recently by Buell in references 6 and 7. Furthermore, these investigators give the necessary analytical expressions for determining the theoretical sound intensity level. The following results on sound attenuation are obtained from reference 6, and the section "Formulation for Geometry of Sound Rays" is a direct quote from that reference.

### Sound Attenuation

In reference 6 an analytical description for hemispherical spreading of sound intensity at a distance is expressed as

$$I = \left(\frac{W}{\pi r^2}\right)\exp(-\alpha r) \qquad (1)$$

where W is the sound power, $a$ is the attenuation coefficient, and I is the intensity at a distance r. The effect of the atmosphere on sound attenuation is obtained by an analysis of the factors that influence the attenuation coefficients. For sound in the atmosphere, the attenuation coefficient is divided into three parts:

$$a = \alpha_1 + \alpha_2 + a3 \qquad (2)$$

where $\alpha_1$ is the classical absorption, $\alpha_2$ is the intermolecular absorption, and $\alpha_3$ is the miscellaneous absorption (e.g., attenuation by fog, clouds, dust, and scattering due to small-scale eddies of wind and temperature).

The classical absorption $\alpha_1$ is made up of four parts:

$$\alpha_1 = \alpha_v + \alpha_c + \alpha_d + \alpha_r \tag{3}$$

where $\alpha_v$ is absorption due to viscosity, $\alpha_c$ is absorption due to conduction heat, $\alpha_d$ is absorption due to molecular diffusion, and $\alpha_r$ is absorption due to radiation of heat.

The attenuation coefficients are discussed in references 8 and 9, but they have been stated here for purposes of completeness and comparison.

Estimates for $\alpha_1$ and $\alpha_2$ have been made in reference 6 with the use of perturbation methods for realistic small-scale and large-scale variations in the atmospheric parameters which affect these coefficients.

The root-mean-square variability of the classical attenuation coefficient $\alpha_1$, at a frequency f of 1 kilocycle and a distance r of 10 km, is given as approximately 0.009 dB for small-scale variations in the atmospheric parameters (variation in the correlation scale parameter of 0.2 km and standard deviation in temperature of 0.3° C) and 0.14 dB for large-scale variations in the atmospheric parameters (standard deviation in temperature of 3.0° C).

The upper limit for the root-mean-square variability of the intermolecular absorption coefficient $\alpha_2$, at a distance r of 10 km, is given as 0.2 dB for small-scale variations in the atmospheric parameters and 5.0 dB for large-scale variations. Over short time periods, $\alpha_2$ is negligible, but over long periods where conditions on the entire ray path are subject to change, the variability of $\alpha_2$ is quite large. The value of $\alpha_2$ depends on a complicated function of the sound frequency and the water vapor content of the air, whereas $\alpha_1$ is mainly temperature dependent and related to frequency in a much simpler manner. From these results, it is noted that the variability of $\alpha_2$ can be much larger than the variability of $\alpha_1$.

## Formulation for Geometry of Sound Rays (Ref. 6)

"The geometry of the sound rays has a pronounced effect on sound intensity estimates. The usual ray tracing methods for an atmosphere consisting of layers that are homogeneous in the horizontal are based on the ray equations

$$\begin{aligned} dx/dt &= c\cos\varphi + u \\ dy/dt &= u \\ dz/dt &= c\sin\varphi \end{aligned} \tag{4}$$

and a variation of Snell's law

$$\frac{c}{\cos\varphi} + u = \frac{c_o}{\cos\varphi_o} + u_o = K \quad \text{(a constant)} \tag{5}$$

where (x,y,z) refer to a "ray point", and
c – speed of sound, u – wind component in the plane of propagation, v – wind component perpendicular to the plane of propagation, $\varphi$ – elevation angle of the phase normal (from horizontal upward), "o" – reference to initial conditions at the source. It is assumed that c, u, v are functions of the vertical coordinate, z. The plane of propagation is taken as the (x,z) plane. It is readily seen from (5) that if the combination c(z) + u(z) equals the value initially on the right-hand side, the value of $\varphi$ is zero and the "ray" is horizontal. When such conditions prevail the ray is bent earthwards and a "direct" sound ray returns to earth.

"The ray equations (4) and Snell's law (5) may be solved explicitly for a layered atmosphere if suitable assumptions are made concerning the variations of c(z) and u(z) within the layers. Since c(z) and u(z) are measured at discrete points, the usual assumption is that values of c(z) and u(z) are linear functions of z between these points. A system of equations for calculating the ray paths under these conditions is given by the system of relations

$$\begin{aligned}
r_2 - r_1 &= -R(\sin\psi_2 - \sin\psi_1), \\
\tan\psi_1 &= c_1 \sin\varphi_1/(c_1\cos\varphi_1 + u_1), \\
\tan\psi_2 &= c_2 \sin\varphi_2/(c_2\cos\varphi_2 + u_2), \\
\cos\varphi_1 &= c_1 \cos\varphi_o/\left[c_o - (u_1 - u_o)\cos\varphi_o\right], \\
\cos\varphi_2 &= c_2 \cos\varphi_o/\left[c_o - (u_2 - u_o)\cos\varphi_o\right], \\
1/R &= \left[(c_2 - c_1)\cos\varphi^* - (u_2 - u_1)\right]/c^*(z_2 - z_1), \\
\cos\varphi^* &= (\cos\varphi_1 + \cos\varphi_2)/2, \\
c^* &= (c_1 + c_2)/2.
\end{aligned} \tag{6}$$

In the above, $r_2$-$r_1$ is the horizontal distance traveled by the ray in crossing the layer from $z_1$ to $z_2$. The subscripts 1 and 2 refer to the bottom and top of this layer, respectively. The total ray path is obtained by adding a string of relations like the first above as the ray passes through successive layers until one is reached in which the ray becomes horizontal. When this occurs the distance traveled is doubled to find the final point where the ray returns to the ground (horizontal). The second and third relations of (6) give the inclination of the ray tangent, $\psi$, at the bottom and top of the layer. The fourth and fifth relations give the inclination of the phase normal, $\varphi$, at the bottom and top of the layer; re-statements of Snell's law, (2). The sixth relation gives the radius of curvature, R, of the ray in the layer. Since the sixth relation is in finite difference form, averaged values

of $\cos\varphi^*$ and $c^*$ are used as given by the last two relations. In the above, the rays are arcs of circles within each discrete layer.

"The distinction between phase normal and ray tangent has been maintained. Inspection of the second and third relations also indicate that $\psi$ and $\varphi$ differ but little. In the atmosphere $c \geq 330$ msec$^{-1}$ while u is at most of the order of 30 msec$^{-1}$ in the lower few kilometers with which we are concerned. In many ray tracing models this distinction is ignored as trivial. Since the elevation angle of the phase normal, $\varphi$, seldom exceeds $20^o$ or so, ray tracing models frequently use a simplified form of Snell's law, $(c+u)/\cos\varphi = (c_o+u_o)/\cos\varphi_o$. In view of the errors in wind measurement, the difference in the results of using this simplification or the more correct form, (5), appears insignificant.

When the rays are computed, the intensity is estimated from the expression

$$I = I_* f \exp(-\alpha r) \tag{7}$$

where $I_*$ is the intensity expected from hemispherical spreading, and the final factor is the attenuation as in (1). The new factor, f, is the "focusing factor", which, for rays returning to the ground, is

$$f = r/\left[\tan\psi_o(\partial r/\partial\psi_o)\right]. \tag{8}$$

The focusing factor expresses nothing more than the area of a ray tube compared with its initial area, i.e., the amount of spreading of the rays. (The ray tube is the locus of sound energy flow while the phase normals are normals to the surfaces of constant phase or wave fronts. The presence of wind forces a distinction between these directions.)

"It is readily seen from (8) that if $\partial r/\partial\psi$ should be zero for a returning ray, the intensity from (7) would become infinite. Such a point (or locus of points) is called a focus. The ray tracing method fails to adequately describe the situation at such points and intensity must be estimated by more sophisticated procedures. These zones, under suitable conditions, are locations of unusually high sound intensity."

## Velocity-of-Sound Profile

The first essential in applying the sound ray tracing technique is an adequate description of the velocity-of-sound profile. The velocity of sound is given by

$$c = 20.0468T^* + \text{Wind component}$$

where $T^*$ is virtual temperature in $^o$K and c is the velocity of sound in m/sec. The wind component is longitudinal to the azimuth of interest and is determined from the wind speed and direction.

In the practical ray tracing equations that are used herein, the velocity of sound with respect to height is considered to be linear over a small height increment or layer. The height increment is taken to be approximately 200 meters as determined by data reduction for the velocity of sound from rawinsonde measurements at 1/2-minute increments of balloon elapse time. The velocity of sound with respect to altitude is the only required data for the ray tracing equations. This system of equations simply traces the ray through the atmosphere by computing the segment of path in each succeeding layer. The path of the ray will either continue to transverse the layers or return to the earth's surface, depending on the slopes of the velocity-of-sound profile or vertical gradients. Two fundamental assumptions underlying ray tracing methods are as follows: (1) the change of speed of sound in a wavelength is small compared with the speed of sound (i.e., $\lambda|\nabla c| << c$); and (2) the variation of the properties of the air over a distance of 1 wavelength must be small $\left(\text{i.e., } \lambda|\nabla^2 c| << |\nabla c|\right)$. Here $\nabla c$ is the gradient of c and $\nabla^2 c$ is its Laplacian. Buell (ref. 6) gives the interpretation that the speed of sound must change smoothly from place to place. These requirements are equally applicable to the wind vector. To assist in determining how detailed the velocity-of-sound profile should be for ray acoustics to be valid, Buell (ref. 6) has evaluated the inequality

$$H >> \left(\lambda^2 \frac{c_0}{4\pi} \frac{dc}{dz}\right)^{1/3} = H^*$$

For the ray method to be valid, H (the depth of the uniform layer) must be much greater than H*. This inequality relationship is illustrated in figure 4, which is taken from reference 6. In reading from figure 4, for a velocity-of-sound gradient dc/dz of 0.008 $sec^{-1}$ and a wavelength $\lambda$ of 50 meters, $H^*$ is 200 meters. The depth of the uniform layer H should be much greater than 200 meters for the ray method to be valid. The merits of this relationship were actually experienced. The MSFC Aerospace Environment Division is responsible for all atmospheric measurements, predictions, and related research for MSFC. The MSFC Test Laboratory is responsible for all static firings and thus the far-field acoustic predictions. In seeking ways to improve far-field sound-intensity estimations, atmospheric measurements were furnished to the Test Laboratory at 15-second rawinsonde time increments which correspond to height increments of about 100 meters. A comparison of the derived sound intensity level with measured sound pressure levels shows greater discrepancies in the results than when atmospheric measurements were furnished at 30-second balloon-elapse-time increments or approximately 200-meter height increments.

From ray acoustic calculations, the vertical gradients of the velocity of sound with respect to the ray patterns can be characterized. Five idealized velocity-of-sound profiles are presented in figure 5. The first profile has a single negative gradient. The rays are deflected upward into the atmosphere, and this produces the condition of no rays

returning. The second profile is known as the "zero" gradient. This condition is required for the inverse square law of sound propagation to be valid.

The third profile has a positive gradient followed by a negative gradient. This condition produces ray concentration and, in practice, has been observed to produce near uniformity in the distance between consecutive intercepts of the ray to the plane tangent to the initial velocity of sound. Thus, uniform rays returning could be an alternate description for this condition. Also, this type of profile closely approximates sound intensity levels derived from the inverse square law.

The fourth profile is characterized by a negative gradient, then a positive gradient, followed by a negative gradient. This condition produces ray focusing. The positive gradient must be such that the velocity of sound in this layer exceeds that at the earth's surface or the initial velocity of sound. The fifth profile produces the combination condition of ray concentration and focusing.

The ray path for idealized velocity-of-sound profiles has been computed with the use of a general-purpose analog computer. The resulting ray profiles are shown in figures 6 to 10 to illustrate specific characteristics of the ray profile patterns for the given velocity-of-sound profiles. The velocity-of-sound gradients are comparable to those which could occur in the atmosphere, but they do not necessarily represent the most severe velocity-of-sound gradients. In a calm atmosphere – that is, with no wind and a dry-adiabatic-lapse rate of $10^{\circ}$ C per 1000 meters of altitude (a temperature decrease of $10^{\circ}$ C per 1000 meters), the resulting velocity-of-sound gradient $dc/dz$ would be $-0.006\ \text{sec}^{-1}$, since a change in temperature of $1^{\circ}$ C produces approximately a 0.6-m/sec change in the speed of sound for the usual ranges of atmospheric temperature near the ground. An adiabatic-lapse rate is a very unstable atmosphere and a condition that would not exist over a very thick layer for a long time without the wind blowing. A reasonably large value for wind shear near the ground over a 1000-meter layer is $0.002\ \text{sec}^{-1}$. This value of wind shear first added to and next subtracted from -0.006 gives the values for the velocity-of-sound gradient of $-0.004\ \text{sec}^{-1}$ and $-0.008\ \text{sec}^{-1}$, corresponding to the downwind and upwind directions, respectively. A reasonably large temperature increase with height up to 500 meters is $20^{\circ}$ C over the United States Plain states during early morning in winter. With this condition, the wind should be calm. The resulting value for $dc/dz$ would be $0.024\ \text{sec}^{-1}$. Large temperature inversions also occur in the Los Angeles area. Using a lapse rate of one-half that of the dry adiabatic lapse and a wind shear of $0.002\ \text{sec}^{-1}$ over 1000 meters produces values for $dc/dz$ of $-0.001\ \text{sec}^{-1}$ and $0.005\ \text{sec}^{-1}$. The general formula for the velocity-of-sound gradient can be expressed as $\frac{\partial T}{\partial z}\frac{a}{\partial T} - \frac{\partial u}{\partial z}$, where $\partial T/\partial z$ is the vertical temperature gradient taken as negative for temperature decreasing with height and positive (an inversion) for temperature increasing with height, where $\frac{\partial c}{\partial T} = \frac{10}{T^{1/2}}$ is the speed-of-sound gradient with $T$ in $^{\circ}$K and $\partial c/\partial T$

in $m\text{-}sec^{-1}\text{-}{}^{o}K^{-1}$, and where $\partial u/\partial z$ is the wind-component gradient, with (+) indicating the downwind direction and (-) indicating the upwind direction. Thus, for no change in wind direction with respect to height and with a temperature decrease of $5^{o}$ C per 1000 meters (a common occurrence), any time the wind speed increases by more than 3 m/sec from the ground to a 1000-meter altitude, a velocity-of-sound inversion in the downwind direction will occur; sound rays will return and the sound intensity level from a sound will be propagated in the downwind direction at higher levels than in the upwind direction.

Figure 6 illustrates the increase in the height of the shadow zone (area to the right of and under the rays) as the velocity-of-sound gradient becomes more negative. Figure 7 shows the ray profiles for an initial zero gradient followed by various negative and positive gradients for higher layers. Figure 8 illustrates the effects of the magnitude and height of the velocity-of-sound inversion on the ray profile pattern. Figure 9 portrays the ray profiles for various negative-positive-negative velocity-of-sound gradients, the size of the shadow zone, and the location of the focal zones. Figure 10 shows various combinations of ray focusing and uniform rays returning for the first two layers being positive gradients with different slopes.

The ordinate and abscissa scales in all the analog computer plots (figs. 6 to 23) can be scaled either up or down by dividing the values on the two scales by the same number, and the resulting ray plots would still be valid. For example, the height (ordinate) and horizontal distance (abscissa) could be divided by any factor up to 10. The upper limit of the scaling factor is determined by the required critical thickness as shown in figure 4.

## Moving Sound Source

The discussion up to this point has been with respect to sound propagation through the atmosphere for a stationary sound source at the ground. The determination of ray acoustics and sound intensity for a moving sound source such as an aircraft or aerospace vehicle in flight is recognized as being very complex. An analytical formulation of the equations necessary to treat this problem has been established by Buell in reference 10. An effort is presently being made to establish the practical equations necessary to calculate sound intensity for a moving source. In the meantime, some interesting ray patterns from an elevated sound source have been obtained on an analog computer and are presented in figures 11 to 23. These analog computer results simulate a sound source above the ground for various velocity-of-sound profiles. In studying these graphs, the reader is to envision that the resulting ray patterns are from the sound of a vehicle at ignition and in flight or, of particular interest to this conference, from the sound of an aircraft on the ground and during take-off and landing. The ray interference or dynamics

of the ray are missing from the simulation; it must be assumed that the method of simulation freezes the motion of the sound source at the indicated altitudes.

It can be noted in figures 11 and 12 that the negative-gradient profiles show no rays returning to the earth's surface for a sound source located on the ground. One would conclude that there would be no apparent problem (noise nuisance or disturbances) for this condition. If the sound source is located above the ground, the extent that rays return depends on the height of the sound source and the gradient of the velocity-of-sound source.

Figures 13 and 14 illustrate the ray patterns for velocity-of-sound profiles with negative-positive gradients and with the sound source at different heights above the ground. Figures 15 and 16 illustrate the ray patterns for velocity-of-sound profiles with positive-negative gradients and with the sound source at different heights. Figures 17 to 23 are presented to illustrate the ray patterns for various three-layered velocity-of-sound profiles with the sound source at various heights.

Another limitation of ray acoustics should be pointed out; in figure 23 with the sound source located at 1 km, the linear layered model for the velocity-of-sound profile yields a shadow zone to the right of the height at 1 km. At 1 km, the derivative of the velocity of sound is discontinuous. Reference 7 points out that if this "corner" were rounded, the area to the right at 1 km would be completely filled with rays. Furthermore, at this local maximum (corner point) there is an infinite discontinuity in $dr/d\psi_0$ and since this calculation of sound intensity is for returning rays, there is reason to be concerned that estimates are due to the linear layered atmospheric model and have little to do with the sound propagation phenomena. In reference 7 methods are proposed for rounding the corner of the velocity-of-sound profile. The ray location and sound intensity estimates from the linear layered model are compared with those from a parabolic model.

## COMPARISON OF CALCULATED AND MEASURED SOUND LEVELS

The ray patterns in themselves do not give an estimate of the sound intensity level to be expected from a given velocity-of-sound profile. Only through experience and the collection of measured sound-pressure-level data can a correlation between the ray patterns and sound intensity level be obtained. However, from theoretical considerations, it can be stated that in those areas where sound rays do return, the sound intensity level may be higher than that predicted by the inverse square law. Conversely, in those areas where no rays return, the sound intensity level will be lower than that predicted by the inverse square law.

Estimates of sound intensity level as a function of distance in all directions from the static test stand (the sound source) must be made for all static firings of large boosters at MSFC and at MSFC-MTF. For this purpose, a number of digital computer programs have been developed during the several years of operations. Only the simplest of these programs will be described and the resulting sound intensity levels compared with measured sound pressure levels from static tests.

The sound intensity level IL is calculated from the expression

$$IL = D + 22 + 10 \log\left(\frac{1}{r}\left|\frac{d\psi_o}{dr}\right| \cot \psi_o\right) \qquad (9)$$

where $D = 10(\log PWL - \log 10) + 130$ and where r is the horizontal distance from the sound source to the incidence of the ray landing on the plane tangent to the earth's surface at the sound source. The terms r and $d\psi_o/dr$ are derived from the velocity-of-sound profile; $\psi_o$ is the angle of the ray leaving the sound source and is incremented at small arbitrary intervals. The overall sound intensity level IL is in units of dB re: $10^{-16}$ watts/cm$^2$.

The characteristics of this equation are as follows:

(1) When the increase of the velocity of sound with respect to height is linear, the argument of the logarithm for small angles $\psi_o$ is approximately $1/r^2$. Therefore, under this condition the inverse square law for sound propagation is approximated.

(2) At a focal point the intensity level is undefined, since at a focal point, $dr/d\psi_o$ is zero. $\left(\text{The condition of } \frac{dr}{d\psi_o} = 0 \text{ defines a focal point.}\right)$

(3) When the velocity of sound decreases at all altitudes, no rays return and hence the intensity level is not determinable. Only for the condition of rays returning can the intensity level be calculated.

It is recognized that the obvious extensions to equation (9) are the inclusion of a term for the directivity of the sound source and a term for atmospheric attenuation. The more complete form would appear as

IL = PWL of source + Directivity of Source + Frequency of source

+ Velocity of sound in the propagating media + Attenuation

The first term, the PWL of source, can be determined theoretically, but it should also be determined from measurements for the particular engine or engine cluster. The second term, directivity of source, is dependent on the configuration of the static test and engine characteristics and should be determined from measurements. The third term, frequency of sound source, should be determined from measurements. The fourth term,

velocity of sound in the propagating media, is controlled by the atmospheric conditions. The fifth term, the attenuation of sound through the atmosphere, is probably the least understood and is an area for considerable basic research using carefully controlled sound and atmospheric measurements. The attenuation term should include molecular attenuation as well as dynamic effects of atmospheric turbulence.

The MSFC-Test-Laboratory estimates of the sound pressure level and directivity for the S-IC and F-1 engine are presented in the following table, where direction is with respect to the center axis of the jet:

| S-IC (a) | | | F-1 engine (east-area stand) (b) | | |
|---|---|---|---|---|---|
| Direction, deg | Sound pressure level, SPL, dB | Xrectivity, dB | Direction, deg | Sound pressure level, SPL, dB | Directivity dB |
| 0 | 140.0 | 2.7 | 0 | 140.5 | 4.6 |
| 10 | 140.4 | 3.1 | 10 | 140.5 | 4.6 |
| 20 | 141.1 | 3.8 | 20 | 141.0 | 5.1 |
| 30 | 142.1 | 4.8 | 30 | 141.0 | 5.1 |
| 40 | 142.5 | 5.2 | 40 | 140.0 | 4.1 |
| 50 | 142.0 | 4.7 | 50 | 140.0 | 4.1 |
| 60 | 140.3 | 3.0 | 60 | 138.0 | 2.1 |
| 70 | 137.8 | .5 | 70 | 135.0 | -.9 |
| 80 | 134.9 | -2.4 | 80 | 133.0 | -2.9 |
| 90 | 132.0 | -5.3 | 90 | 134.0 | -1.9 |
| 100 | 129.8 | -7.5 | 100 | 132.0 | -3.9 |
| 110 | 128.2 | -9.1 | 110 | 130.5 | -5.4 |
| 120 | 127.2 | -10.1 | 120 | 129.5 | -6.4 |
| 130 | 126.5 | -10.8 | 130 | 128.5 | -7.4 |
| 140 | 125.6 | -11.7 | 140 | 127.5 | -8.4 |
| 150 | 124.2 | -13.1 | 150 | 126.0 | -9.9 |
| 160 | 122.5 | -14.8 | 160 | 124.0 | -11.9 |
| 170 | 122.3 | -15.0 | 170 | 122.5 | -13.4 |
| 180 | 122.1 | -15.2 | 180 | 120.5 | -15.4 |

[a]Average power level of 210.9 dB and average sound pressure level of 137.3 dB (based on measurements at distance of 610 meters from source).

[b]Average power level of 203.5 dB and average sound pressure level of 135.9 dB (based on measurements at distance of 305 meters from source).

Figure 24 shows a comparison of the sound intensity level, the inverse-square-law result, and the measured overall sound pressure level for a static firing of Saturn I on February 27, 1963, at 1648 CST. For the azimuth 45° east of north (fig. 24), the sound intensity levels compare favorably with the overall-sound-pressure-level measurements. The sharp rise in the sound-intensity-level curve at a 16-km distance is attributed to a focal point (or focal zone). The sound intensity level is infinite; however, inasmuch as finite yet small increments of $\psi_c$ are used, the computed unsteady levels are unrealistically high in the neighborhood of a focal point. When the sound intensity levels are displayed as in figure 25, the focal areas are characterized by high intensity-level values and large gradients. For figure 25, the sound intensity levels were derived for 36 azimuths and isacoustic lines (lines of constant sound intensity level) were drawn.

These sound-intensity-level estimates are with respect to a flat earth surface. Hills which are high enough to intercept the ray path and local wind and temperature gradients over the hills can conceivably modify the resulting sound intensity level. (Compare the ray profile in fig. 26 with the intensity levels in fig. 24.)

The test results from a static firing of Saturn I on March 13, 1964, at 1633 CST are presented for a 45° azimuth in figure 27. Two focal zones are indicated, one at 13 km and another at 22 km. The sound-intensity-level estimates are within 5 dB of the measured sound pressure levels.

The results from two static firings are presented to illustrate the rapid change over short time periods in the sound ray patterns in area extent, the variability of sound-intensity estimates, and the difficulty in predicting the velocity-of-sound profile. The results from a static firing on October 23, 1964, are shown in figures 28 to 31, and the results from a static firing on November 23, 1964, are presented in figures 32 to 35.

Figure 28 shows the areas in which sound rays returned and the sound intensity levels based on a 12-hour forecast of wind and virtual temperature valid for October 23, 1964, at 1640 CST. This prediction of sound rays and intensity levels can be compared with the results from the rawinsonde measurements presented in figure 30. In addition, intensity levels based on rawinsonde measurements taken at 1539 CST – that is, taken 61 minutes before firing time – are presented in figure 29. The ray pattern based on rawinsonde measurements at firing (fig. 30) can be compared with the ray pattern based on rawinsonde measurements 34 minutes later (fig. 31). Although the change in ray pattern is rather systematic, the sound-intensity-level estimate at a given point varies considerably. The 12-hour prediction (fig. 28) is judged to be very good.

Figures 32 to 35 present the sequence of sound ray patterns and sound intensity levels based on the 12-hour atmospheric prediction valid for November 23, 1964, at 1640 CST (the static firing time) and the results based on rawinsonde measurements

taken at T-45, T-0, and T+36 minutes. A no-change extrapolation of the ray pattern from the rawinsonde measurements for T-45 minutes to a T-0 pattern would have produced poorer results than the original 12-hour forecast. The ray pattern for T+36 minutes is in closer agreement with the 12-hour prediction than the T-0 pattern. No claim is made that the predictions of the velocity-of-sound profile which yield such close agreement in ray patterns are this accurate in general.

The MSFC Test Laboratory has, on occasions, rescheduled static firings on the basis of predicted velocity-of-sound profiles. At present, the entire test operation is based on atmospheric measurements and predictions furnished by the MSFC Aerospace Environment Division, whereas in former times, the acoustical horn was used to augment the expected far-field sound intensity level.

A comparison of the sound intensity level and the sound-pressure-level measurements obtained from a measuring program conducted at the MSFC Missippippi Test Facility in 1962 and 1963 is presented. The sound source was an acoustical horn which at that time had a sound-power-level capability up to 6000 watts. (At MSFC in Huntsville, the acoustical horn had sound-power-level capability up to 178 000 watts.) The atmospheric measurements were obtained from the rawinsonde GMD-1B system. By using these simultaneous measurements of sound pressure levels and atmospheric measurements from which sound intensity levels have been calculated, a comparison is made between the sound intensity level and sound pressure level. The best agreement between the sound pressure level and the sound intensity level within a ±500-meter distance was chosen for this comparison. These data are summarized in figures 36 and 37 for two different atmospheric conditions. In figure 36, a comparison is made between sound intensity level and the measured sound pressure level for the atmospheric conditions which produce uniform rays returning. The standard regression error is 5.2 dB. In figure 37, the intensity levels for all conditions of rays returning, including focal conditions, are compared with the sound-pressure-level measurements. The standard regression error here is 7.1 dB. Contributing to the regression errors are (1) theoretical assumptions for the intensity level calculations, (2) errors in atmospheric and acoustic measurements, and (3) time and space variability of atmospheric parameters. The major criticism of this comparison is the manner in which the best agreement between the sound intensity level and the sound-pressure-level measurements was selected. In view of the influence of small errors in the velocity-of-sound profile on the sound intensity level and short time variations in the wind flow, the comparison made in this manner may not be entirely invalid. Plots were made of the difference between the sound pressure level and the sound intensity level as a function of distance from the sound source, and no apparent correlation with respect to distances from the sound source was noted. Therefore, it is concluded that under similar situations at MTF, practical results from the sound-intensity-level calculations can be used to predict the expected sound pressure

level as a function of distance from the source for the Saturn V and larger vehicle boosters.

Through improved atmospheric measurements and sound-intensity-level programs and with the Saturn booster as the sound source, there have been some improvements in the statistical estimates of the differences between sound intensity level and sound-pressure measurements. However, large improvements cannot be expected because of the inherent variability of the wind and temperature profile from which the velocity-of-sound profile is derived. With the use of realistic interval correlation coefficients to relate the random variability of temperature and the wind vector profile, a Monte Carlo simulation was performed in reference 7 to determine the standard deviations of sound intensity level for ray returns for distances from 5 to 50 km. Three degrees of atmospheric variability were used: (1) small variability (time period less than 1 hour); (2) moderate variability (time period of 4 to 6 hours); and large variability (time period of 8 to 12 hours). Systematic changes in the wind and temperature that might be caused by morning radiation temperature inversion and frontal passages were excluded from this consideration. The modal values of the standard deviations from this simulation, when not less than 20 percent of the rays failed to return, were 2.5 to 5.0 dB for all three variability scales.

## STATISTICAL ANALYSIS

Far in advance of actual static tests, sometimes several years in advance, the planning engineers must know the influence of pertinent atmospheric conditions on the facility operations. Two approaches may be used to show the relationship between atmospheric variables and engineering design parameters used in planning a facility. One approach is to take the summarized statistics of atmospheric variables and attempt to derive the influence of these variables on the facility. The monthly mean values of temperature and the wind components and their standard deviations for discrete altitude levels were used in reference 11 to arrive at an estimated frequency at which sound generated from the vehicle would be intensified by quadrant areas. Estimates based on such a procedure should be viewed with caution because the correlations between atmospheric variables with respect to altitude should be considered. Often the required correlation values are not immediately available and must be derived.

It is proposed that a better procedure is to (1) derive the required analytical equations relating the atmospheric variables to the required engineering design parameters, (2) use the individual atmospheric measurements to calculate the engineering parameters for design, and (3) summarize these data in a statistical manner.

This method will not only yield a more efficient estimate of the frequency of the occurrence for the particular parameters of interest, but will often be more economical than computing all the required correlations between the atmospheric variables themselves.

This procedure was followed in constructing figures 38 to 43, which are discussed in the following paragraphs. The ray acoustics and intensity levels were calculated by using the individual rawinsonde measurements taken at MSFC at 1630 CST for January and July of 1962 and 1963. The frequency at which the rays return along each of 36 azimuths was computed.

From figure 38 it can be seen that 100 percent of the rawinsonde measurements for January 1962 and January 1963 at 1630 CST produced rays returning somewhere along the 90° azimuth (east of MSFC); along the 270° azimuth (west of MSFC), only 35 percent of the rawinsonde measurements produced rays returning. Similarly, the frequency of rays returning along the 90° and 270° azimuths for July of 1962 and 1963 at 1630 CST are 60 percent and 18 percent, respectively (see fig. 39). Any time rays returned, the sound pressure level from a static test could be expected to be higher than for the condition of no rays returning. Therefore, charts like these for all months of the year would assist a site planning group in placing the test facility at such a location in the community that the likelihood for disturbances due to anomalous sound propagation resulting from test operations would be a minimum. From a knowledge of the prevailing wind direction over Huntsville up to a 3000-meter altitude, the conclusion that the frequency at which rays returned would be higher toward the east than toward the west could be reached. However, the relative frequency of rays returning for the two directions could not be stated. This information has already been used to advantage by a facility planning group at MSFC in the design and layout of the Saturn V static test stand.

A knowledge of the frequency of rays returning anywhere along an azimuth leaves much to be desired for detailed facility planning. A knowledge of the frequency of rays returning within a given area would be more useful. Since the computations of rays returning were by necessity carried out in a polar coordinate system, unit area is designated by 5-km intervals along (and ±5° on either side of) each of the 36 azimuths. The frequencies at which at least one ray returned within a 5-km interval along each of the 36 azimuths were computed. These frequencies are summarized for January and July in figures 40 and 41. The highest insistence of rays returning is east of the static test stand out to a distance of 10 km. It is noted that Army headquarter buildings and industrial plants are located in the first 5 km east of the static test stand. Between 10 and 20 km east of the test stand is located a recently constructed residential area. The business district of Huntsville is located northeast of the static test stand between 10 and 15 km. Thus it is obvious that an engineering effort should be made to minimize the

sound pressure level produced by the boosters in these directions. During July the pattern of the frequency of rays returning is more circular than that for January. The boundaries of the Redstone Arsenal are approximated by a circle of 10-km radius. Thus, it is observed that there is less than a 25-percent chance that rays will return outside the, arsenal boundaries during July.

Because of the directivity effects, the static test stand should be orientated such that the sound pressure level is minimized east and northeast of the static test stand. This conclusion is valid for the existing community. However, since the construction of the S-IC static test stand, a multimillion dollar jet airport has been built just west of the arsenal boundaries. This poses the problem of predicting the future growth of a community surrounding the static test area.

The question that still must be answered is how frequently will atmospheric conditions be such that anomalous sound propagation will cause disturbances to the outlying community during static tests of the Saturn V or other vehicles yet to be built. By using the theoretical intensity-level equation as described previously, the frequencies at which the intensity levels equal or exceed 110 dB for the condition of rays returning have been calculated. It must be realized that no attenuation factor has been included in these calculations; therefore, the frequencies at which the intensity level exceeds 110 dB will be higher than they should be. Figures 42 and 43 indicate that when rays return, there is a high probability the sound generated by the Saturn V will equal or exceed 110 dB out to distances of 20 km.

It is realized that the available data sample is small for the detailed statistical treatment as presented in figures 38 to 43. The techniques or methods of statistical analysis should prove helpful in determining statistics of acoustical parameters for other locations and related problems. However, the statistical analysis of the acoustical parameters should be performed with the use of individual atmospheric measurements obtained at the specific localities.

## OPERATION OF ATMOSPHERIC MEASURING SYSTEM

At MSFC an atmospheric measuring system has been in operation since October 1961. The equipment consists of two GMD-1B units with the capabilities of GMD-2 units. Through a switching mechanism, the GMD-2 can be operated automatically to produce punched cards for azimuth and elevation angles, ratios of temperature and humidity ordinates, and slant range at 5-second intervals of balloon flight time. This latter system is known as the ADP system - that is, the automatic data processing system (ref. 12). Predictions up to 36 hours in advance of static tests are required for the wind speed, direction, and virtual temperature profiles. Weather charts by facsimile and weather

teletype information are received to assist in making these predictions. From 6 hours prior to static test time until actual static test time, rawinsonde measurements are performed at 1- to 2-hour intervals. Until recently, the MSFC Test Laboratory made sound-pressure-level measurements with the use of the acoustical horn as a sound source. If through these measuring techniques and predictions the sound pressure level in the community appears to be too high – that is, equal to or greater than 110 dB, the test conductor cancels the static firing and reschedules the test when the atmospheric conditions are more favorable.

## CONCLUDING REMARKS

Many methods can be used to obtain numerical solutions to the differential equations for sound rays. Although there are recognized limitations in ray acoustics, instructive and useful results indicating the effects of atmospheric refraction can be obtained from ray acoustic methods. The several analog computer solutions illustrate the ray paths propagated through a linear layered model of the velocity-of-sound profile and quantitatively give a relative comparison of sound pressure levels that may result from a sound source located on the ground and in the air. Through a systematic study of the propagation of sound through the atmosphere, analytical techniques have been developed for determining the far-field sound intensity level resulting from a sound source located on the ground that compares very favorably with sound pressure levels measured under field-test and operational conditions. The major requirement is the velocity-of-sound profile, which can be obtained from atmospheric measurements of the wind and virtual temperature profiles. Prediction of the sound intensity levels for a test operation requires a forecast of the wind and virtual temperature profiles. A study is in progress to develop sound-intensity estimation techniques for a moving sound source. A satisfactory analytical model for determining far-field sound-intensity estimates for a moving sound source would be most useful in acoustic studies related to aircraft in flight. The statistical methods for ray refraction for particular locations of interest could be useful in planning future airports and land usage near the existing airports.

## REFERENCES


1. Dorland, Wade D.: Far-Field Noise Characteristics of Saturn Static Tests. NASA TN D-611, 1961.

2. Cox, Everett F.; Plagge, H. J.; and Reed, J. W.: Meteorology Directs Where Blast Will Strike. Bull. Amer. Meteorol. Soc., vol. 35, no. 3, Mar. 1954, pp. 95-103.

3. Perkins, Beauregard, Jr.; Lorrain, Paul H.; and Townsend, William H.: Forecasting the Focus of Air Blasts Due to Meteorological Conditions in the Lower Atmosphere. Rep. No. 1118, Ballistic Res. Lab., Aberdeen Proving Ground, Oct. 1960.

4. Rothwell, P.: Calculation of Sound Rays in the Atmosphere. J. Acoust. Soc. Amer., vol. 19, no. 1, Jan. 1947, pp. 205-221.

5. Heybey, Willi H.: Theoretical Aspects of Planar Sound Propagation in the Atmosphere. MTP-AERO-62-72, NASA George C. Marshall Space Flight Center, Oct. 23, 1962.

6. Buell, C. Eugene: Variability of Sound Propagation Prediction Due to Atmospheric Variability. NASA CR-61160, Kaman Aircraft Corp., Jan. 1967.

7. Buell, C. Eugene: Comparison of Two Methods for Estimating Sound Intensity. NASA CR-61187, Kaman Nuclear, Jan. 1968.

8. Bishop, Dwight E.; and Franken, Peter A.: Propagation of Sound From Airport Ground Operations. Conference on Progress of NASA Research Relating to Noise Alleviation of Large Subsonic Jet Aircraft, NASA SP-189, 1968. (Paper No. 30 herein.)

9. Guest, Stanley H.; and Adams, Bert B.: Methods of Determining the Excess Attenuation for Ground-to-Ground Noise Propagation. Conference on Progress of NASA Research Relating to Noise Alleviation of Large Subsonic Jet Aircraft, NASA SP-189, 1968. (Paper No. 31 herein.)

10. Buell, C. Eugene: Variability of Sound Propagation Prediction Due to Atmospheric Variability. KN-68-698-4 (Contract No. NAS8-11348), Kaman Nuclear, June 28, 1968.

11. Anon.: Acoustical Considerations in the Planning and Operation of Launching and Static Test Facilities for Large Space Vehicles. Phase I. BBN-884 (Contract NAS8-2403), Bolt, Beranek, and Newman, Inc., Dec. 11, 1961.

12. Turner, R. E.: Radiosonde Data System. Instr. Control Syst., vol. 40, Apr. 1967, pp. 99-100.

ESTIMATED ACOUSTICAL POWER LEVEL FOR SEVERAL AEROSPACE VEHICLES

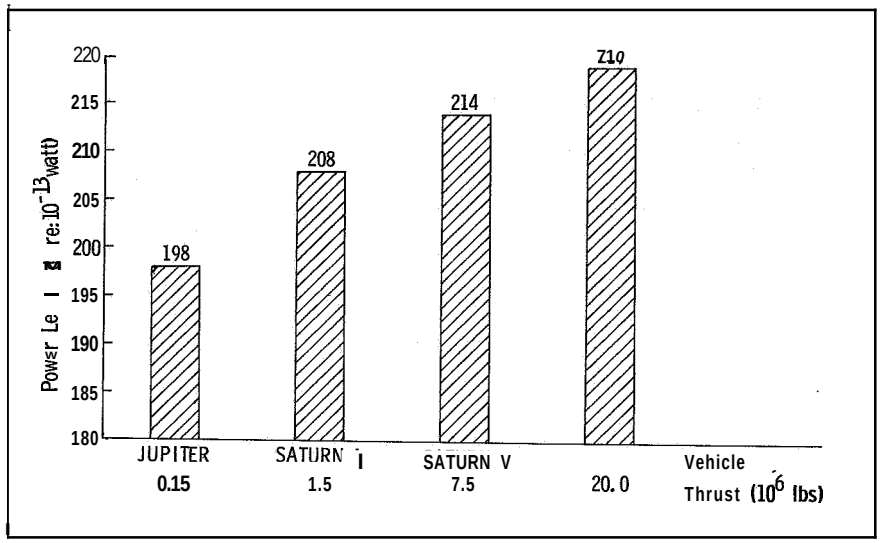


Figure 1

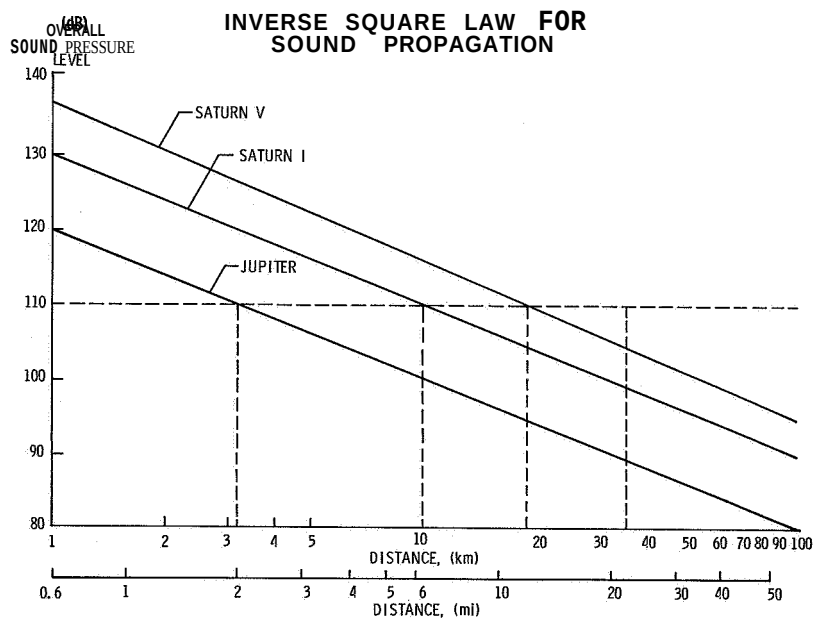


Figure 2

RADII TO CRITICAL SOUND PRESSURE LEVEL (110 dB) FOR SATURN I AND SATURN V USING INVERSE SQUARE LAW

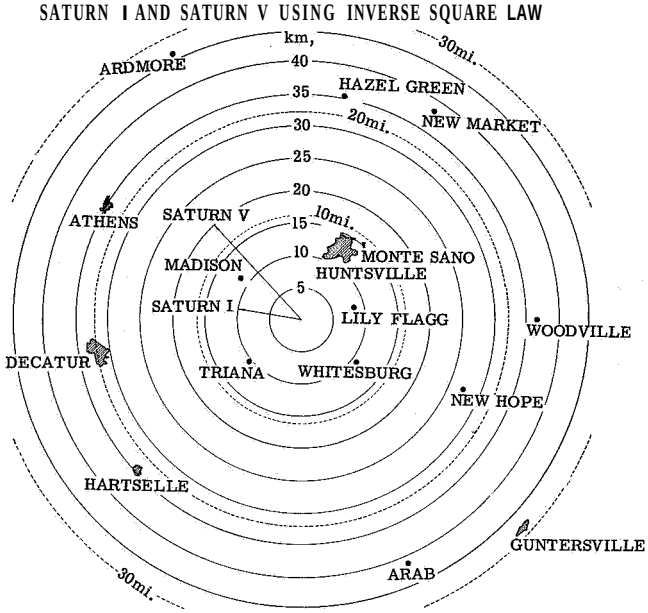


Figure 3

GRAPH OF $H^* = \left(\lambda^2 \frac{c_o}{4\pi} \frac{dc}{dz}\right)^{1/3}$

[$\lambda$ = WAVELENGTH; $c_o$ = INITIAL SPEED OF SOUND; $\frac{dc}{dz}$ = GRADIENT OF SPEED OF SOUND ABOVE UNIFORM LAYER; f = FREQUENCY]

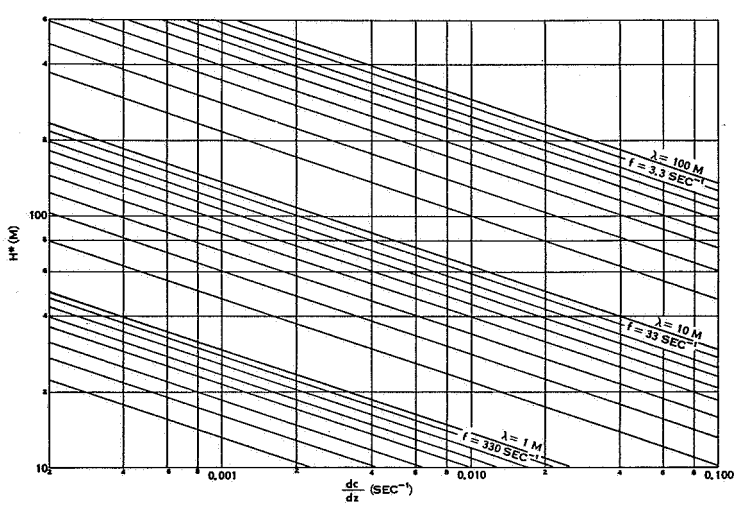


Figure 4

# VELOCITY-OF-SOUND **PROFILES** AND RAY PATTERNS

1. 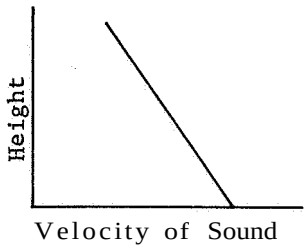


Rays are deflected upward (no rays returning)

2. 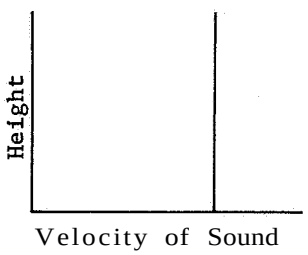


Rays returning uniformly in all directions (Inverse–Square–Law Condition)

3. 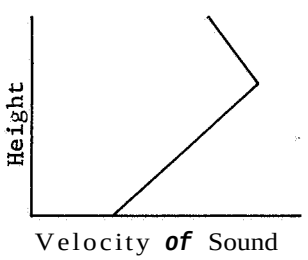


Uniform rays returning (ray concentration)

4. 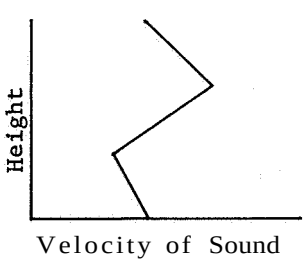


Ray focusing

5. 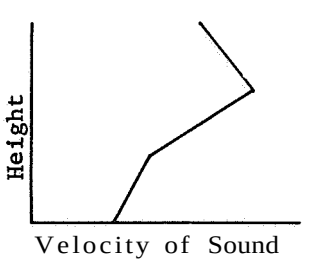


Ray concentration and focusing

**Figure** 5

ANALOG RAY TRACE SOLUTIONS SHOWING VARIOUS NEGATIVE GRADIENT PROFILES

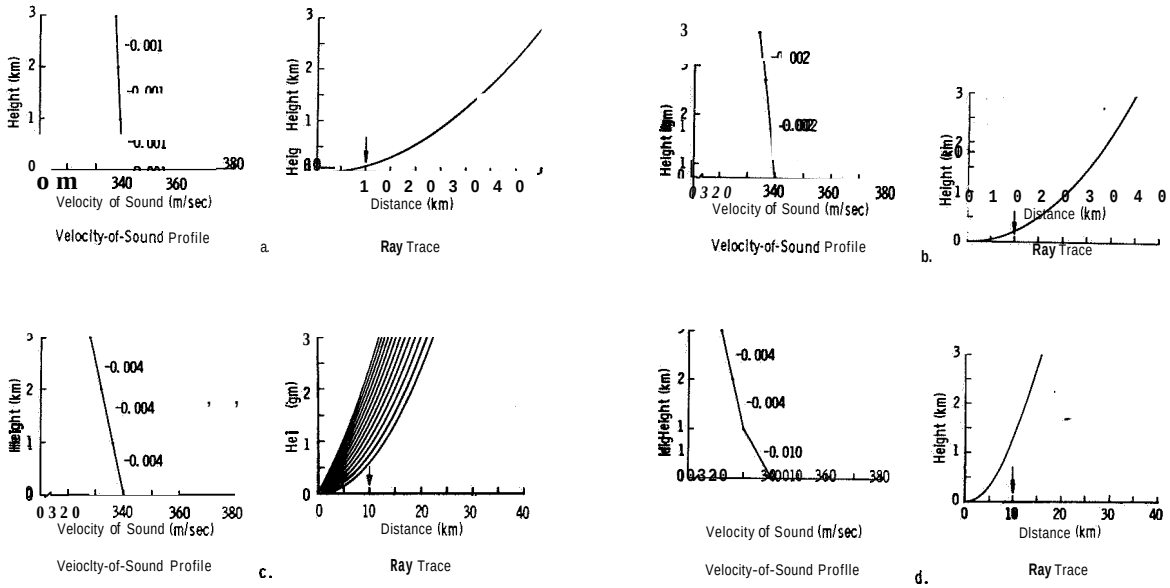


Figure 6

ANALOG RAY TRACE SOLUTIONS SHOWING VARIOUS ZERO-POSITIVE-NEGATIVE AND ZERO-NEGATIVE-POSITIVE GRADIENT PROFILES

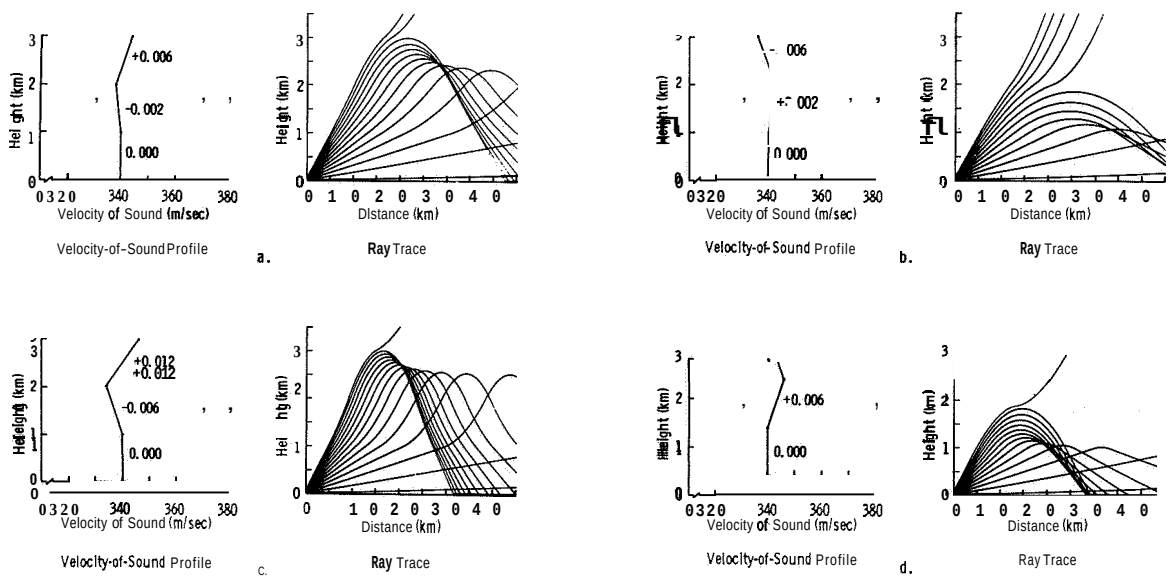


Figure 7

ANALOG RAY TRACE SOLUTIONS SHOWING VARIOUS POSITIVE-NEGATIVE GRADIENT PROFILES

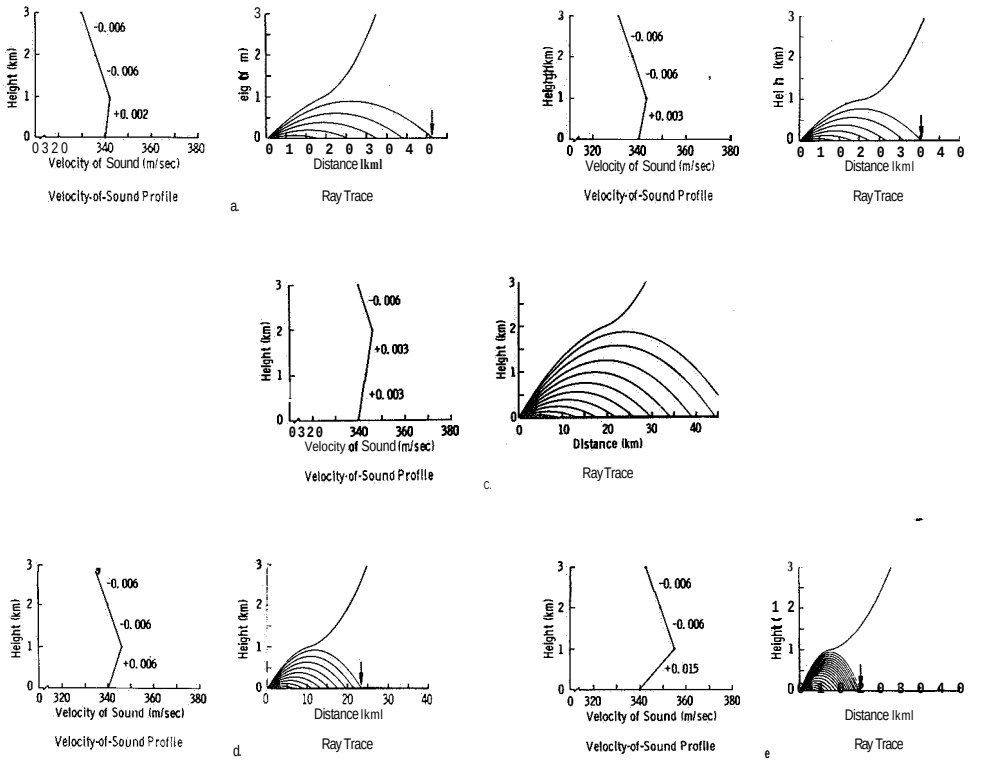


Figure *8*

ANALOG RAY TRACE SOLUTIONS SHOWING VARIOUS NEGATIVE-POSITIVE-NEGATIVE GRADIENT PROFILES

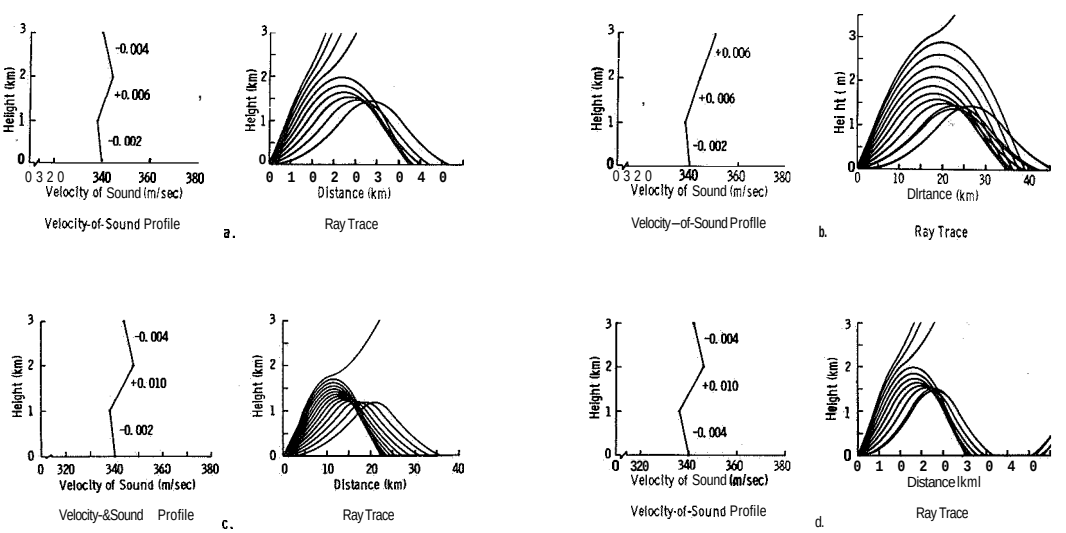


Figure *9*

ANALOG RAY TRACE SOLUTIONS SHOWING VARIOUS POSITIVE-POSITIVE-NEGATIVE GRADIENT PROFILES

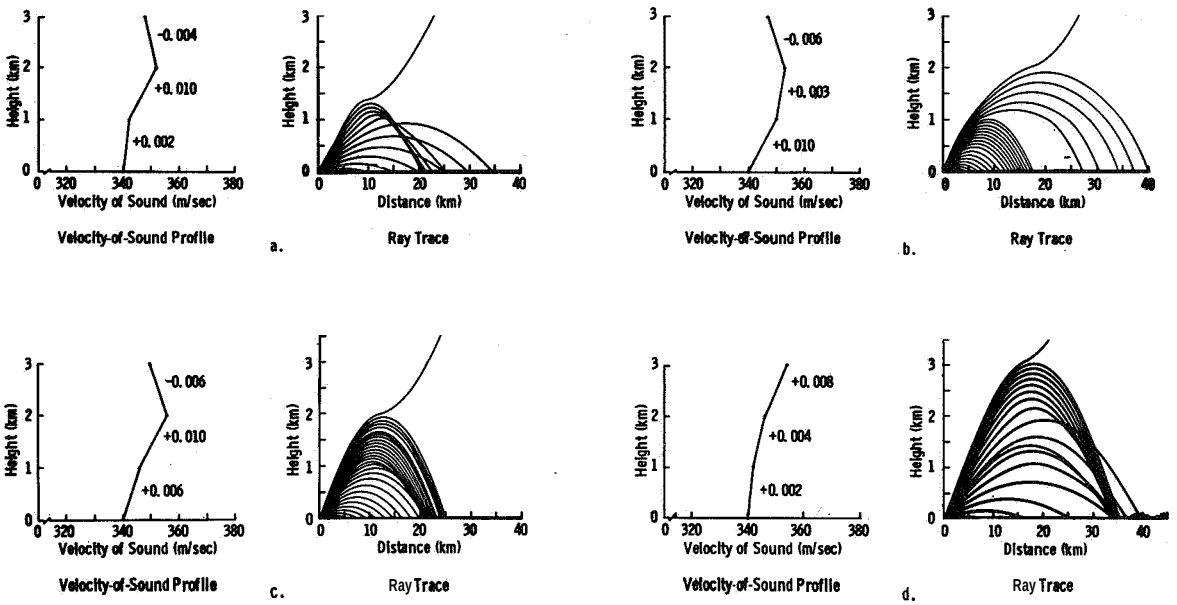


Figure 10

## ANALOG RAY TRACE SOLUTIONS FOR SOUND SOURCE AT HEIGHTS OF 0, 1, AND 2 km (STRONG NEGATIVE GRADIENT)

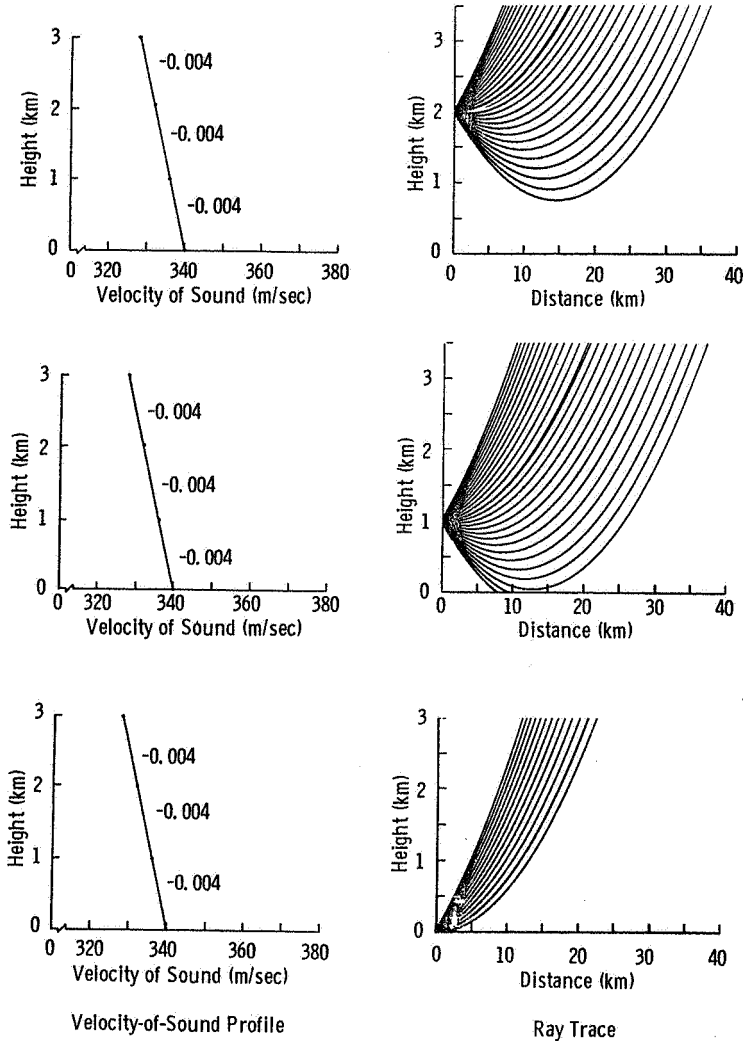


Figure 11

## ANALOG RAY TRACE SOLUTIONS FOR SOUND SOURCE AT HEIGHTS OF 0, 1, AND 2 km (NEGATIVE GRADIENT)

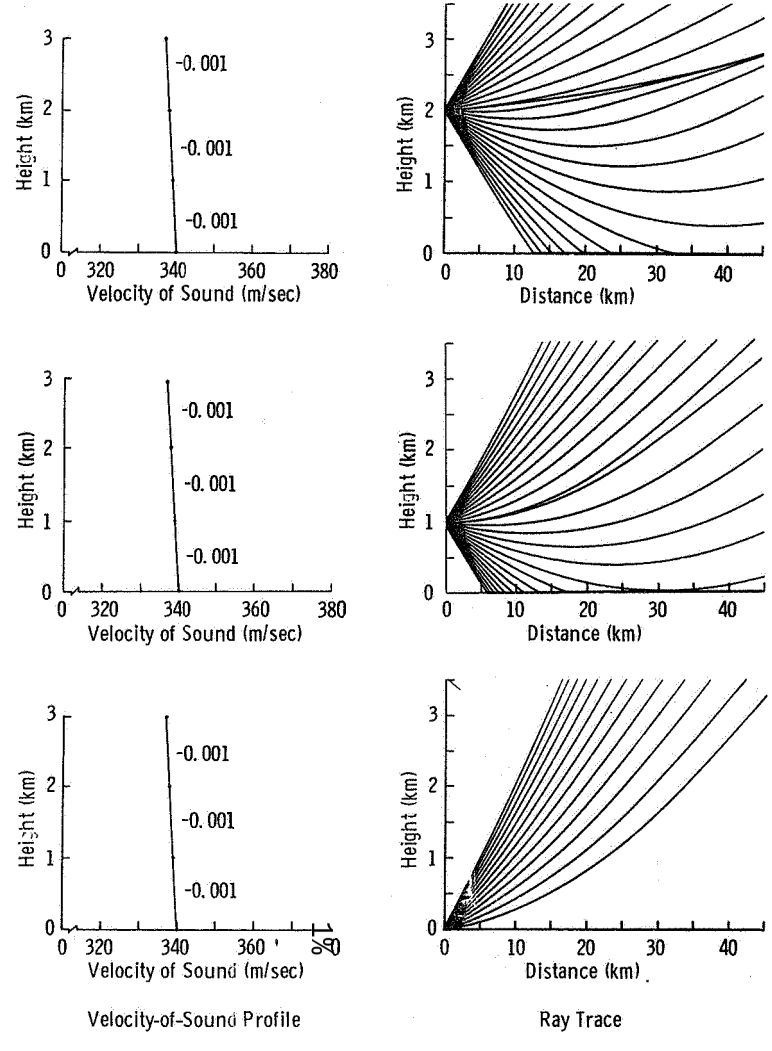


Figure 12

## ANALOG RAY TRACE SOLUTIONS FOR SOUND SOURCE AT HEIGHTS OF 0, 1, AND 2 km (STRONG NEGATIVE-POSITIVE GRADIENT)

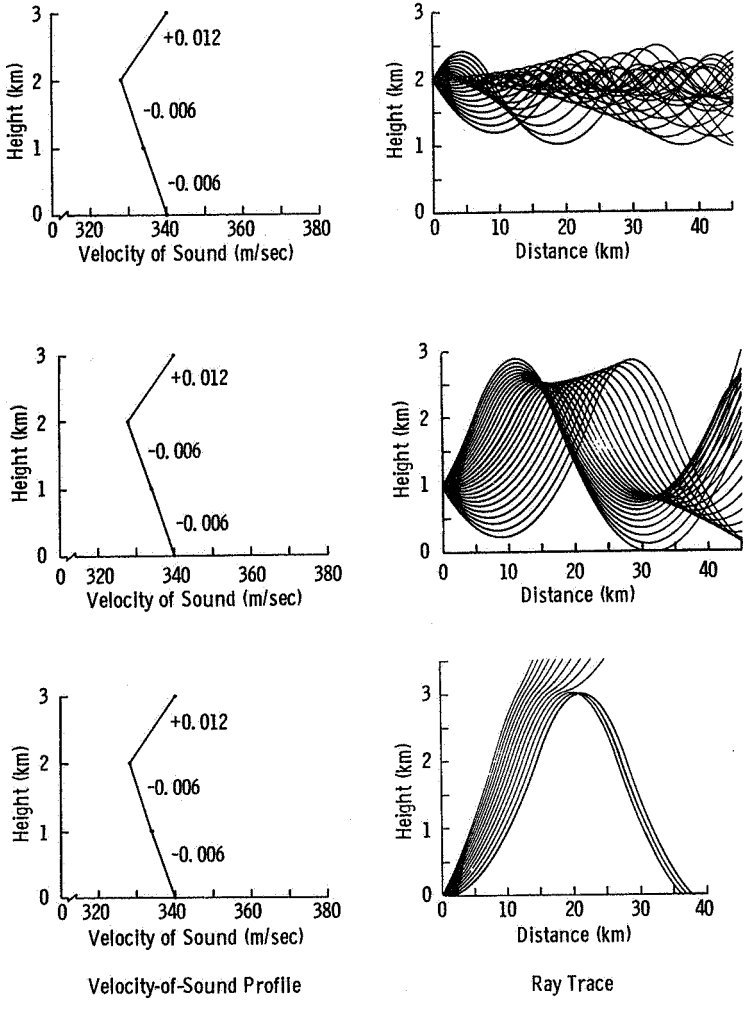


Figure 13

## ANALOG RAY TRACE SOLUTIONS FOR SOUND SOURCE AT HEIGHTS OF 0, 1, AND 2 km (NEGATIVE-POSITIVE GRADIENT)

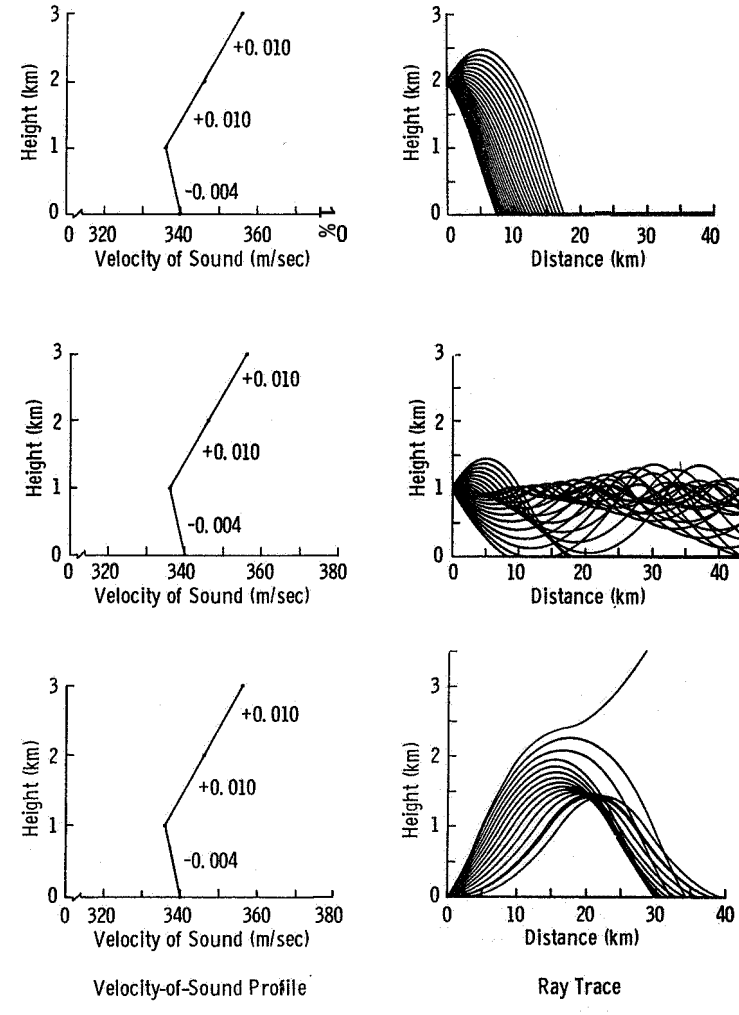


Figure

## ANALOG RAY TRACE SOLUTIONS FOR SOUND SOURCE AT HEIGHTS OF 0, 1, AND 2 km (POSITIVE-NEGATIVE GRADIENT)

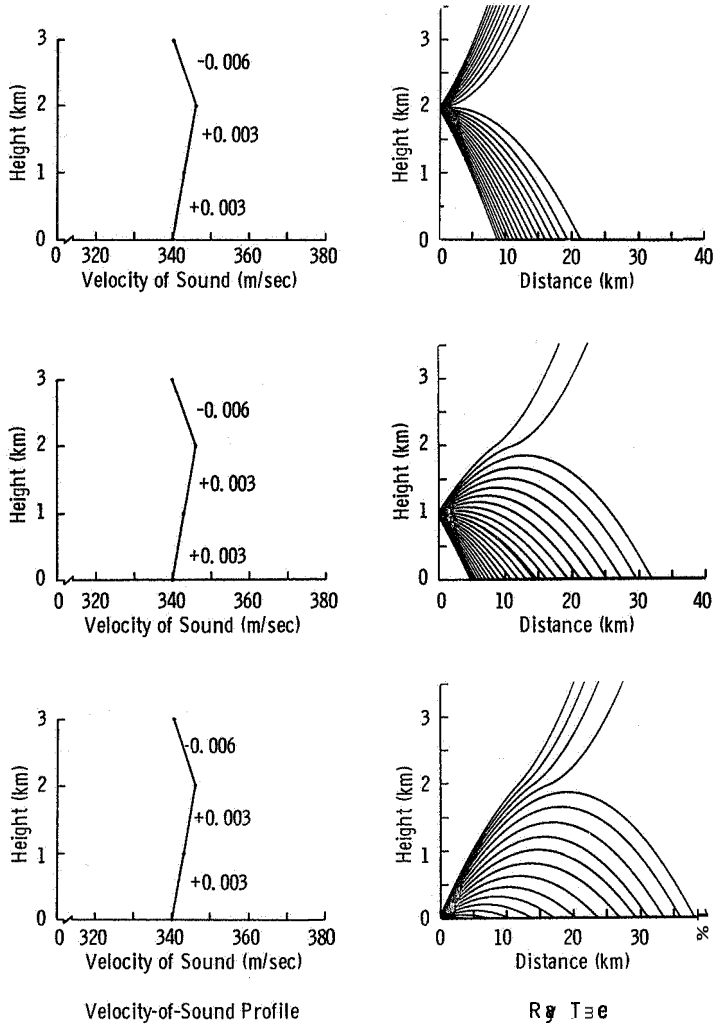


Figure 15

## ANALOG RAY TRACE SOLUTIONS FOR SOUND SOURCE AT HEIGHTS OF 0, 1, AND 2 km (STRONG POSITIVE-NEGATIVE GRADIENT)

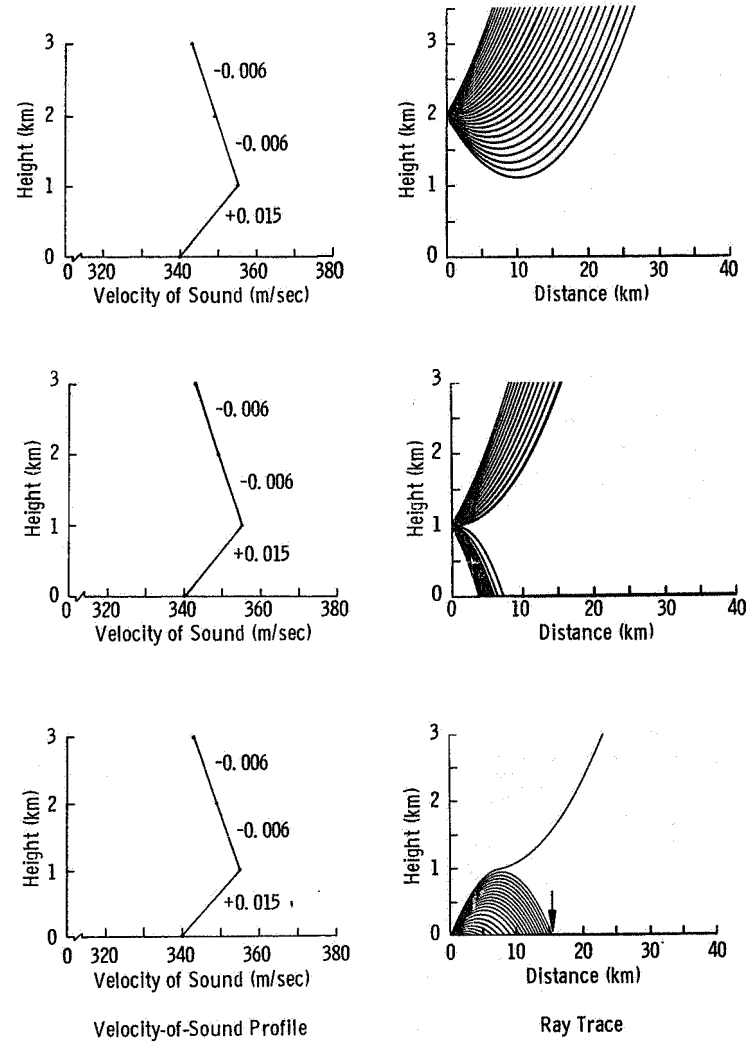


Figure 16

## ANALOG RAY TRACE SOLUTIONS FOR SOUND SOURCE AT HEIGHTS OF 0, 1, AND 2 km (NEGATIVE-POSITIVE-NEGATIVE GRADIENT)

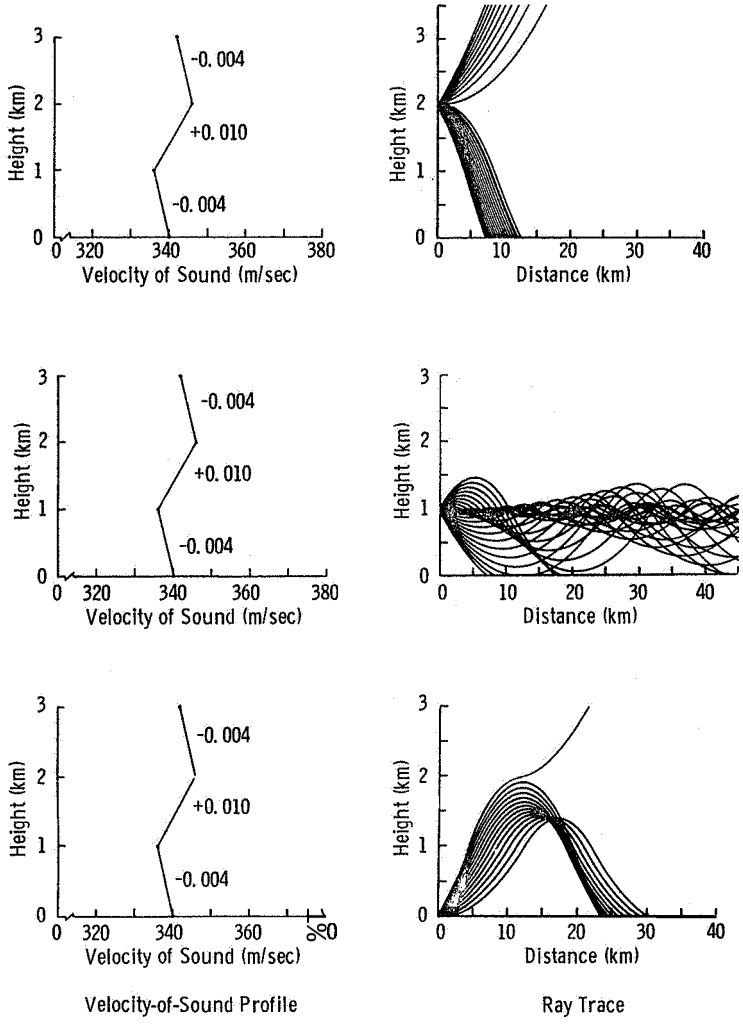


Figure 17

## ANALOG RAY TRACE SOLUTIONS FOR SOUND SOURCE AT HEIGHTS OF 0, 1, AND 2 km (STRONG NEGATIVE-NEGATIVE-POSITIVE GRADIENT)

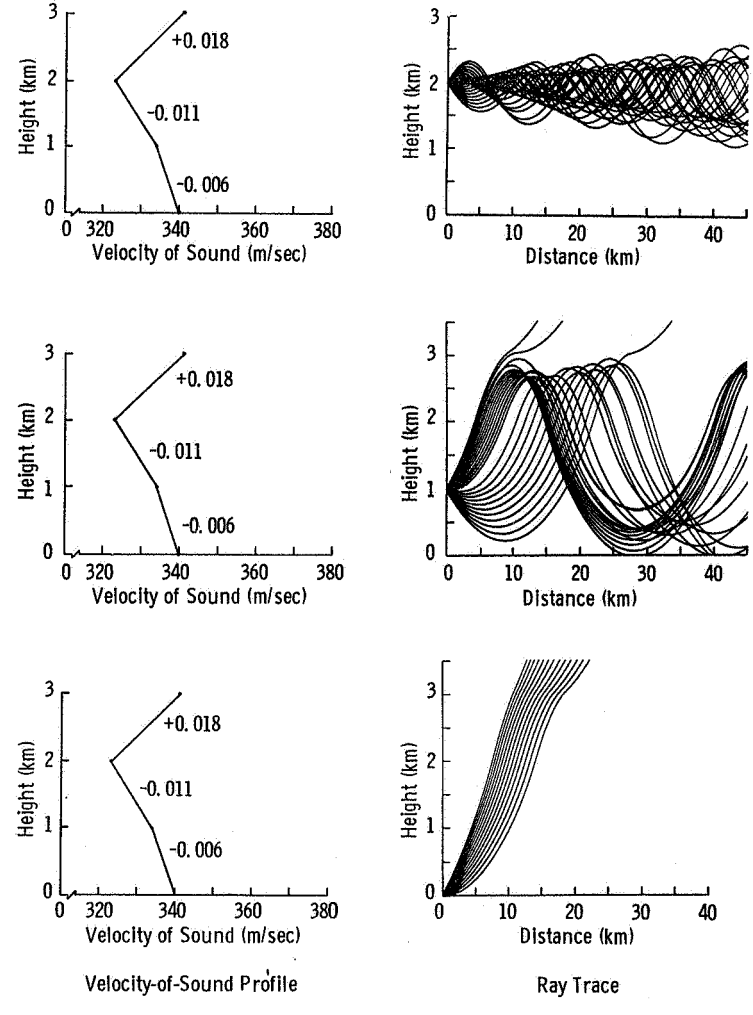


Figure 18

## ANALOG RAY TRACE SOLUTIONS FOR SOUND SOURCE AT HEIGHTS OF 0, 1, AND 2 km (ZERO-NEGATIVE-POSITIVE GRADIENT)

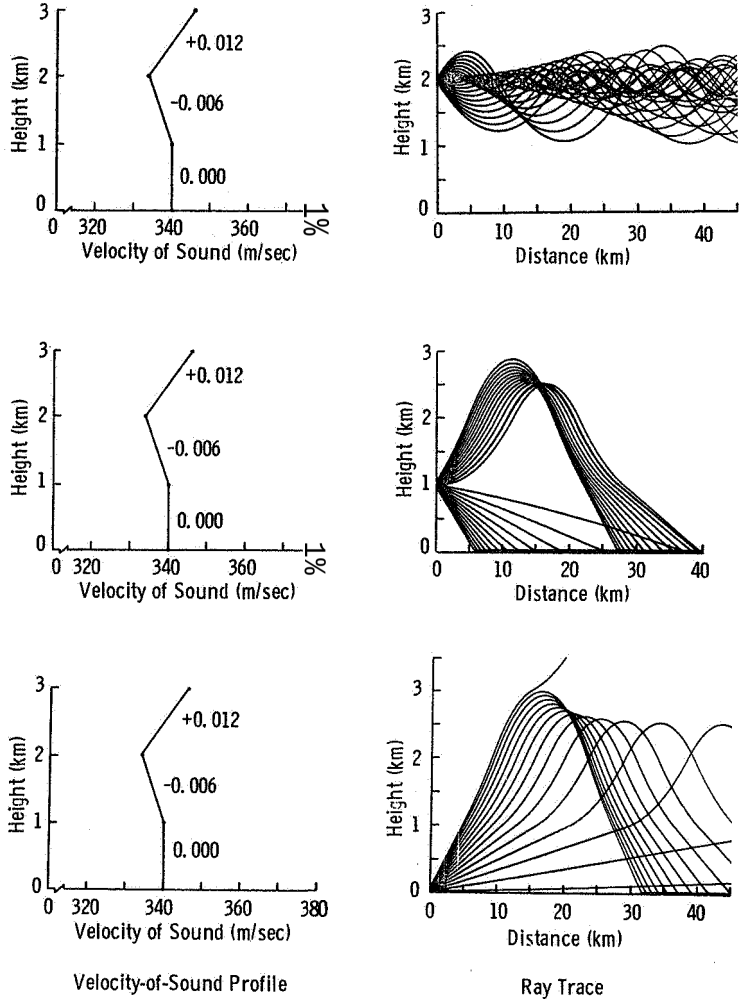


Figure 19

## ANALOG RAY TRACE SOLUTIONS FOR SOUND SOURCE AT HEIGHTS OF 0, 1, AND 2 km (ZERO-POSITIVE-NEGATIVE GRADIENT)

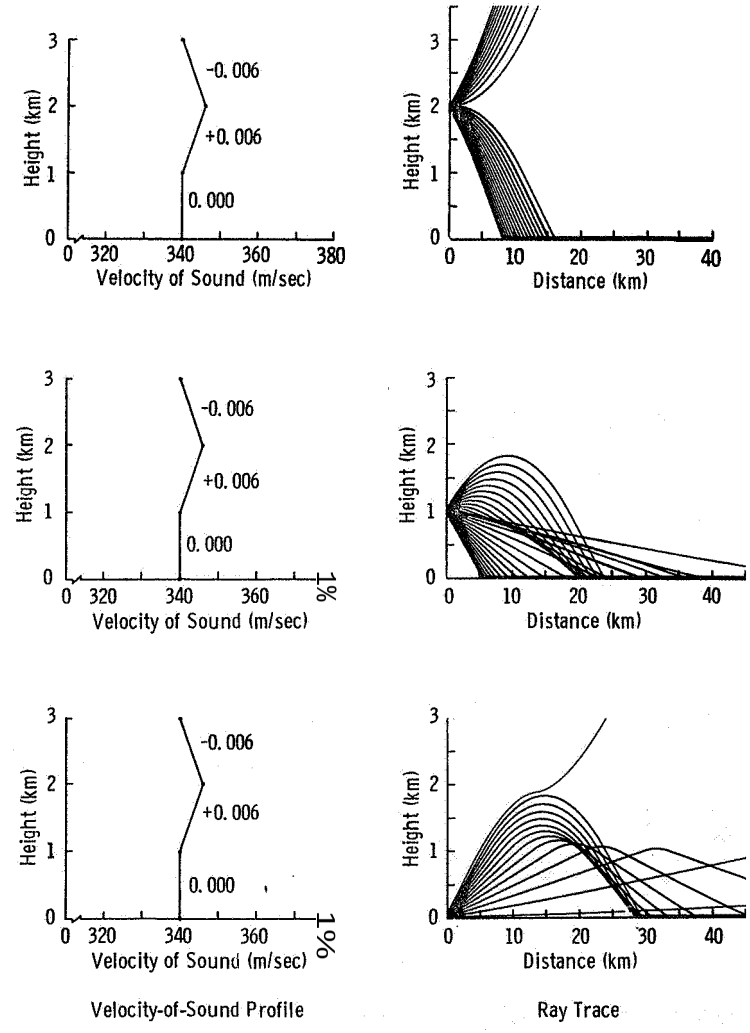


Figure 20

## ANALOG RAY TRACE SOLUTIONS FOR SOUND SOURCE AT HEIGHTS OF 0, 1, AND 2 km (POSITIVE-POSITIVE-NEGATIVE GRADIENT)

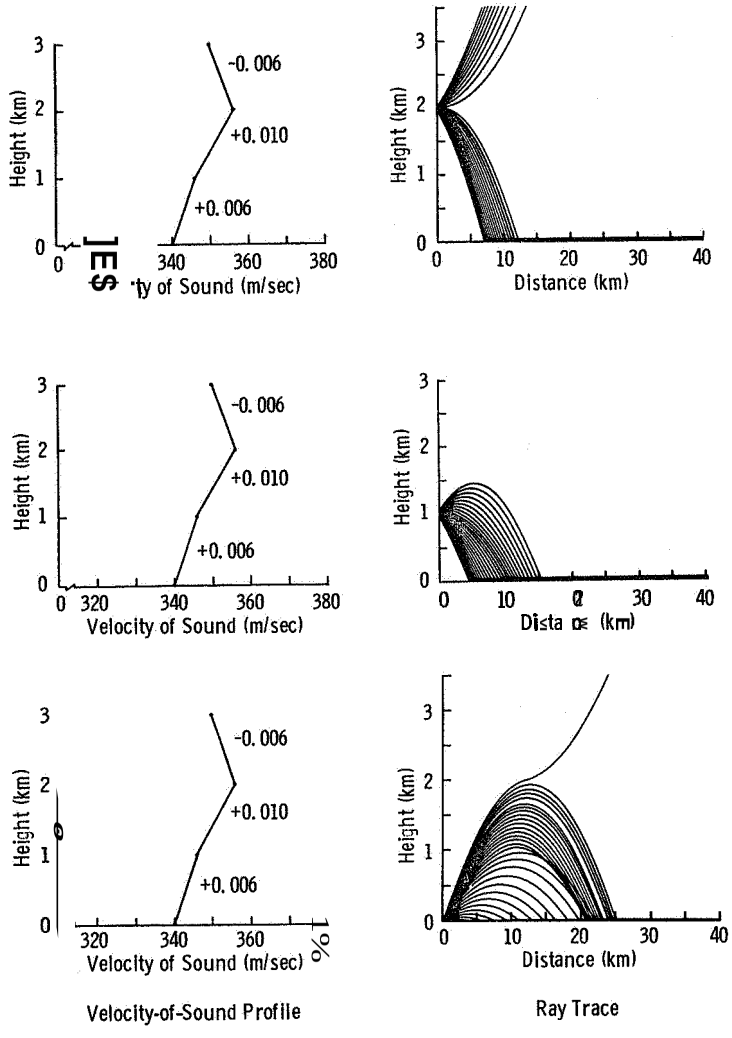


Figure 21

## ANALOG RAY TRACE SOLUTIONS FOR SOUND SOURCE AT HEIGHTS OF 0, 1, AND 2 km (STRONG POSITIVE-POSITIVE-NEGATIVE GRADIENT)

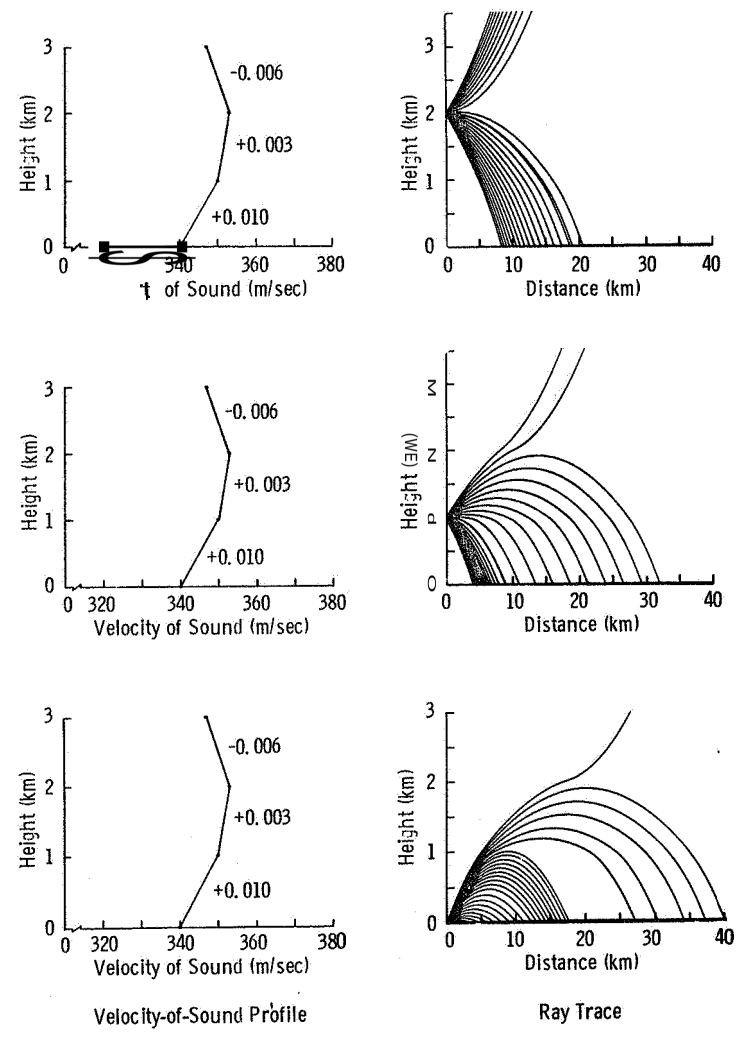


Figure 2

## ANALOG RAY TRACE SOLUTIONS
## FOR SOUND SOURCE AT HEIGHTS OF 0, 1, AND 2 km
## (STRONG POSITIVE-NEGATIVE-POSITIVE GRADIENT)

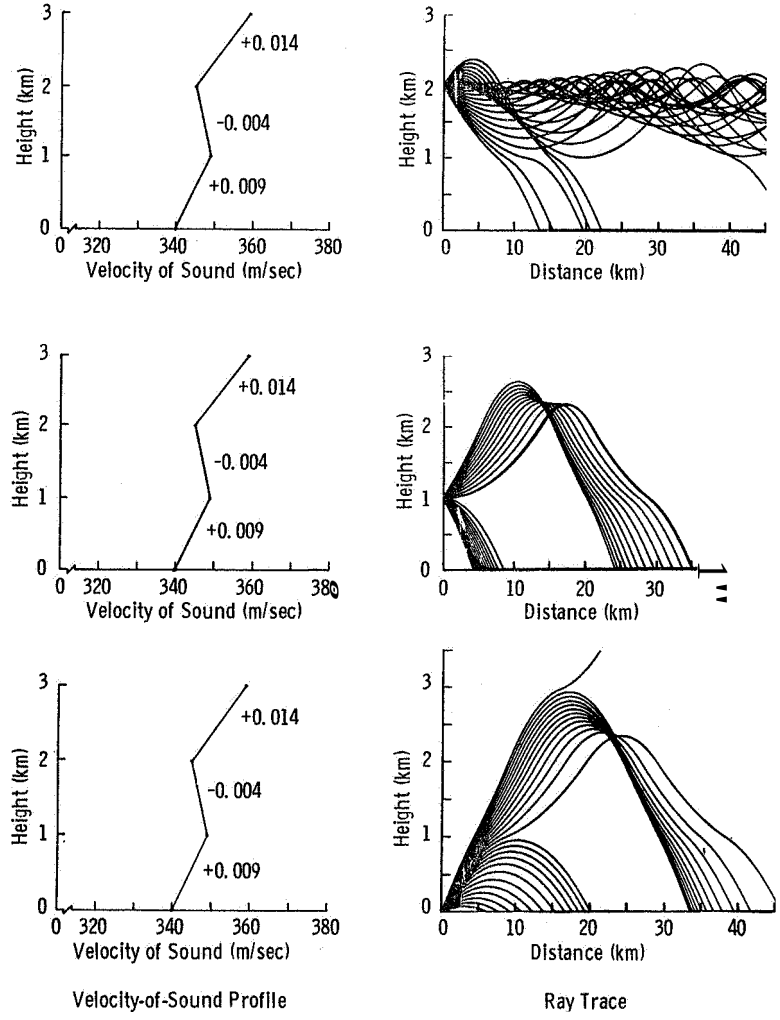


Figure 23

# COMPARISON OF SOUND INTENSITY LEVEL WITH MEASURED SOUND PRESSURE LEVEL FOR STATIC TEST, FEBRUARY 27, 1963, 1648 CST, LONG 45° AZIMUTH (HUNTSVILLE, ALABAMA)

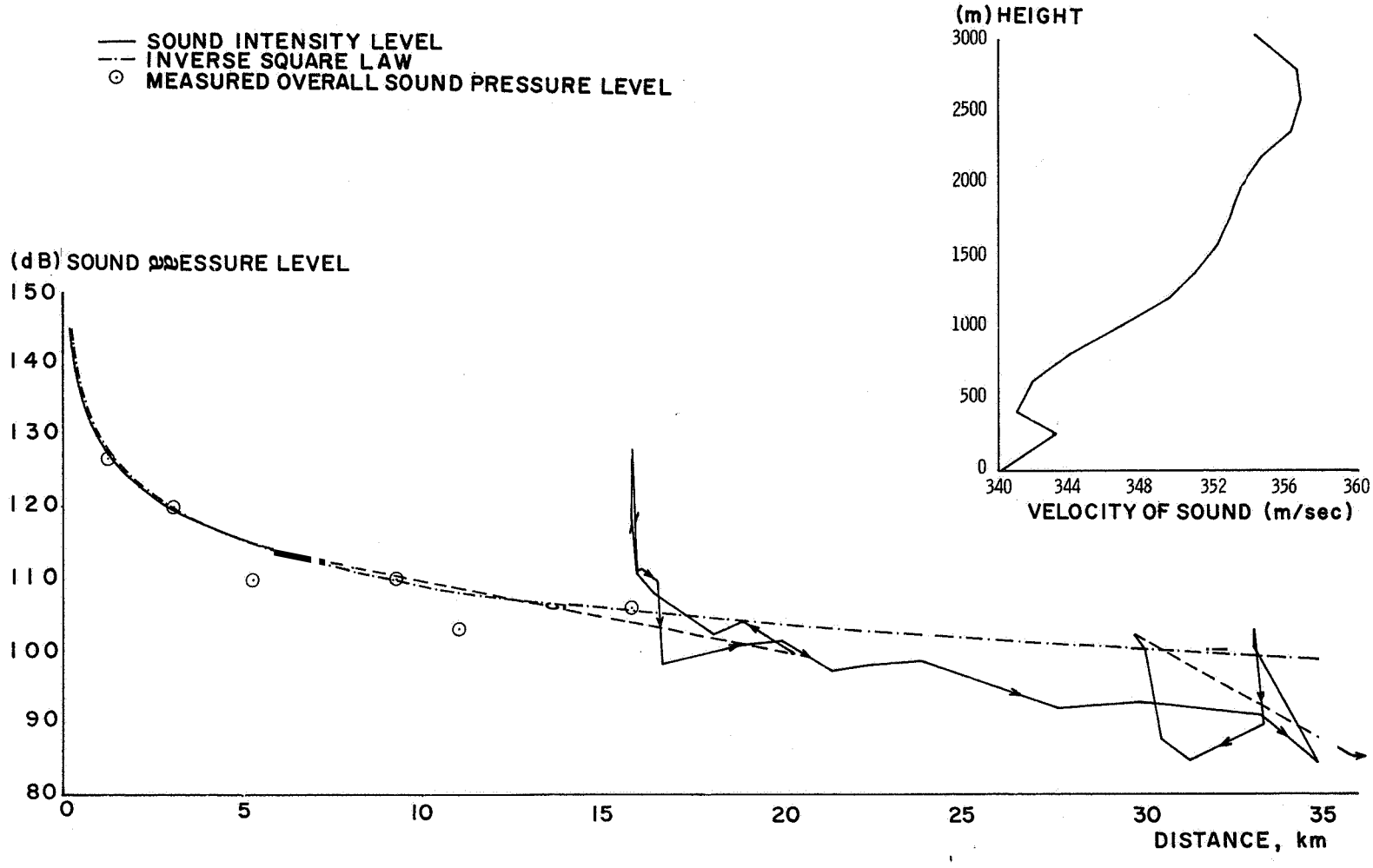


Figure 24

## SOUND INTENSITY LEVELS IN VICINITY OF MSFC STATIC TEST FEBRUARY 27, 1963,1648 CST

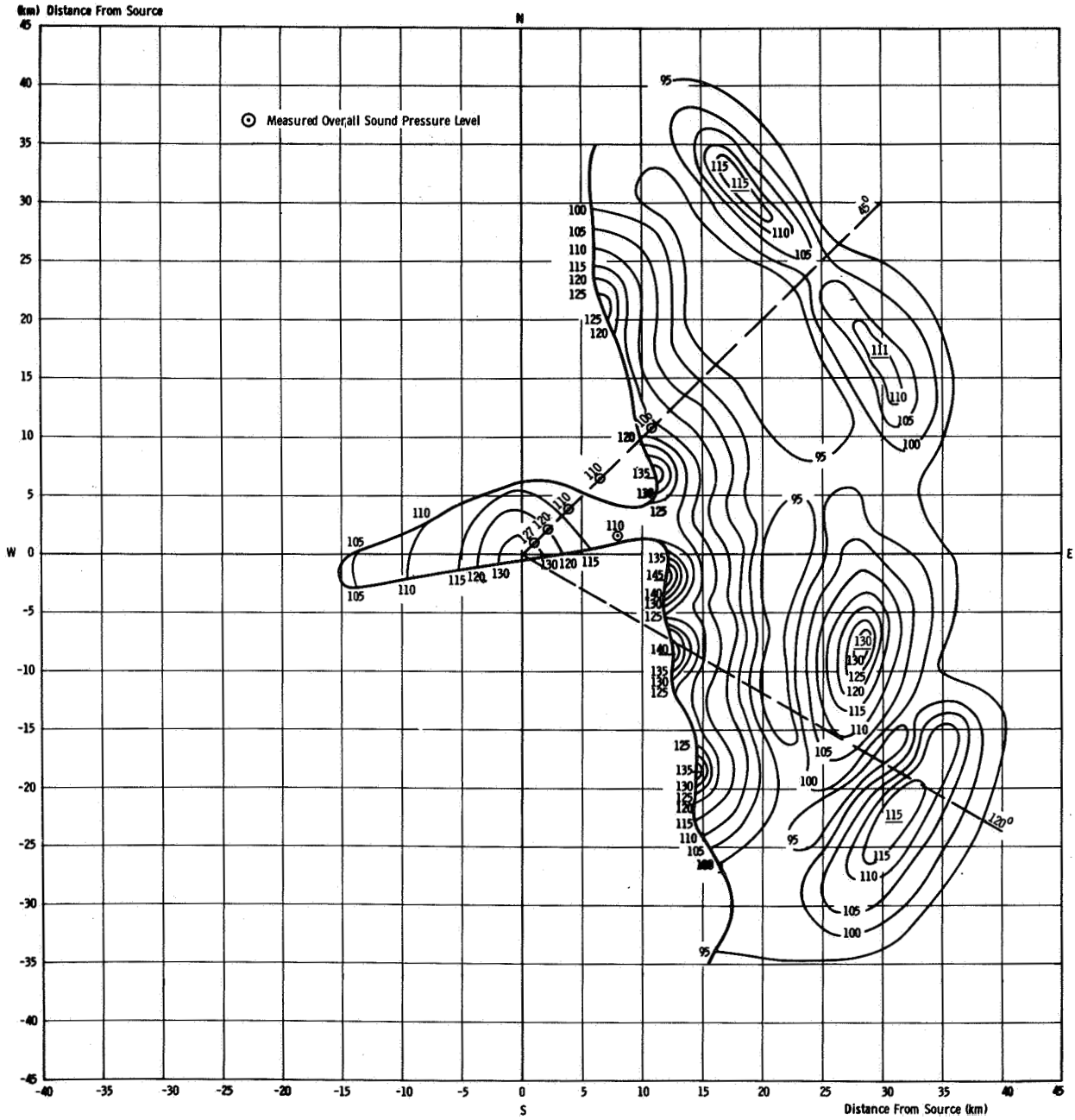


Figure 25

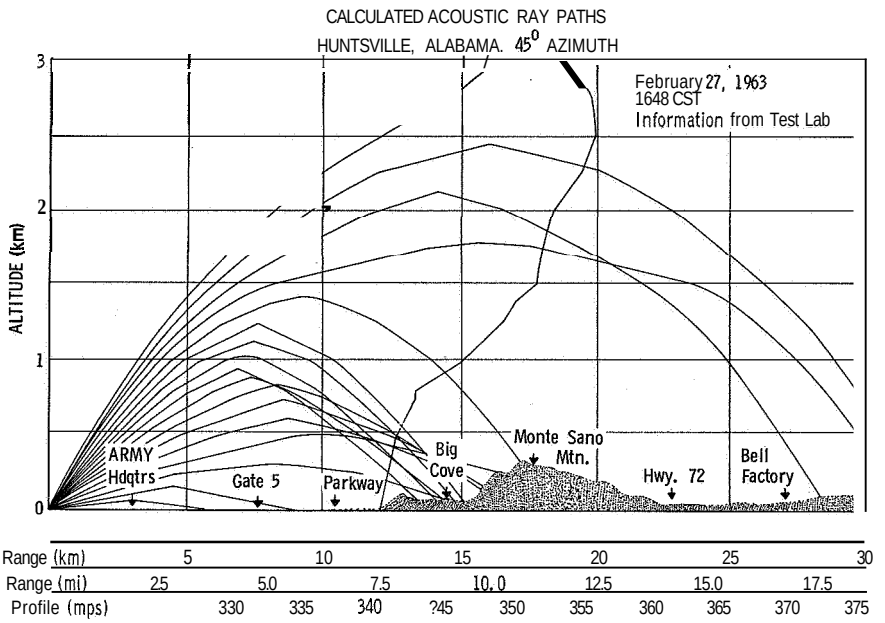


Figure 26

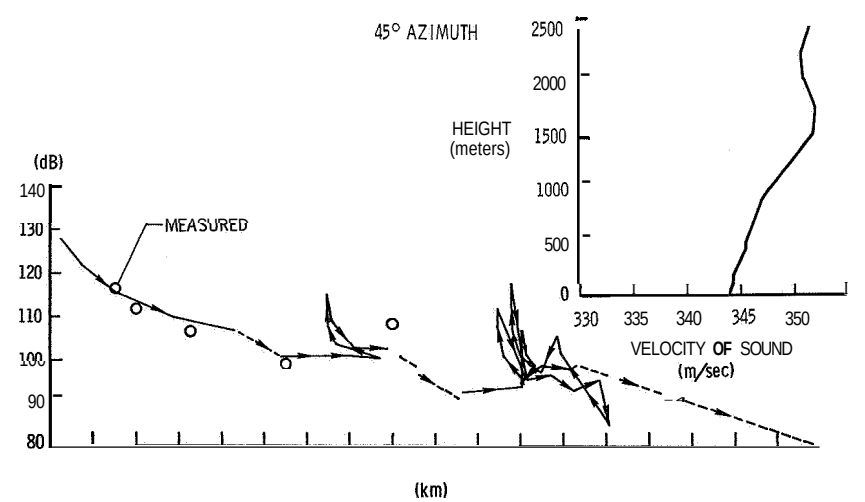


Figure 21

## SOUND INTENSITY LEVELS

**12-HOUR ATMOSPHERIC PREDICTION**

**(FOR STATIC FIRING: OCT. 23, 1964, 1640 CST)**

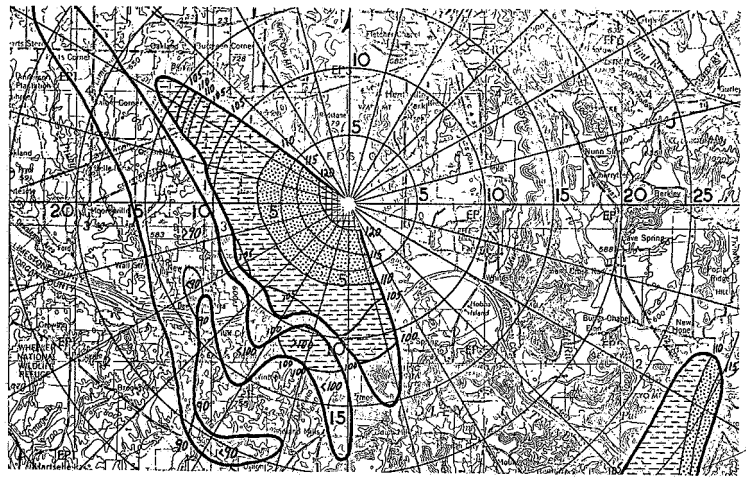

Figure 28

## SOUND INTENSITY LEVELS

**RAWINSONDE MEASUREMENTS; T-61 MINUTES**

**(FOR STATIC FIRING: OCT. 23, 1964)**

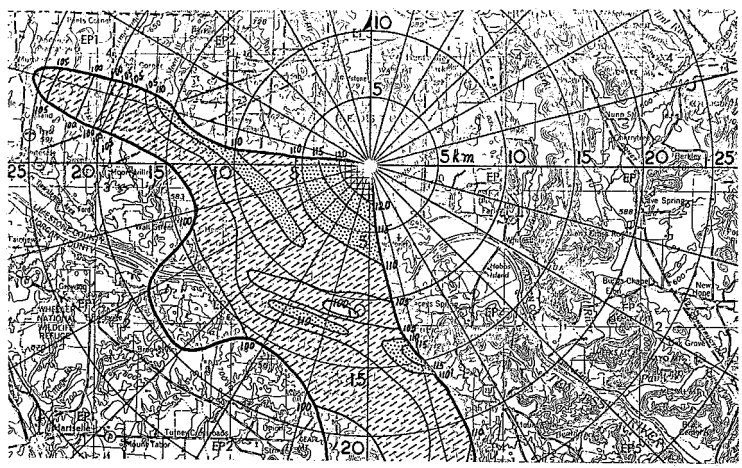

Figure 29

## SOUND INTENSITY LEVELS

RAWINSONDE MEASUREMENTS; T-0 MINUTES

(FOR STATIC FIRING: OCT. 23, 1964)

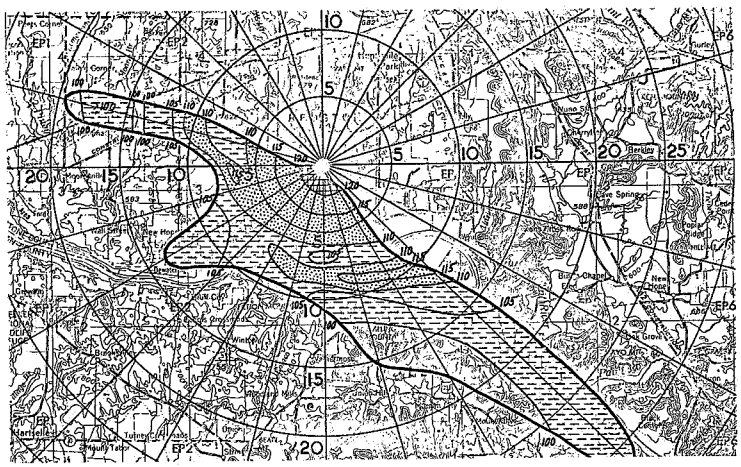

Figure 30

## SOUND INTENSITY LEVELS

RAWINSONDE MEASUREMENTS; T+34 MINUTES

(FOR STATIC FIRING: OCT. 23, 1964)

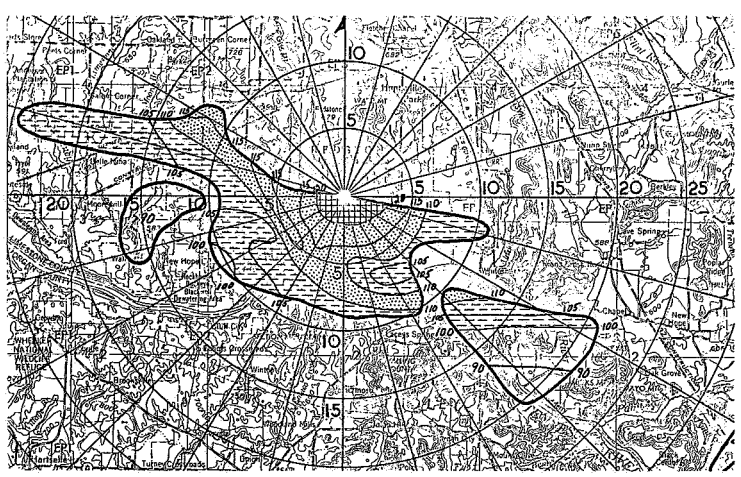

Figure 31

## SOUND INTENSITY LEVELS

12-HOUR ATMOSPHERIC PREDICTION

(FOR STATIC FIRING: NOV. 23, 1964, 1640 CST)

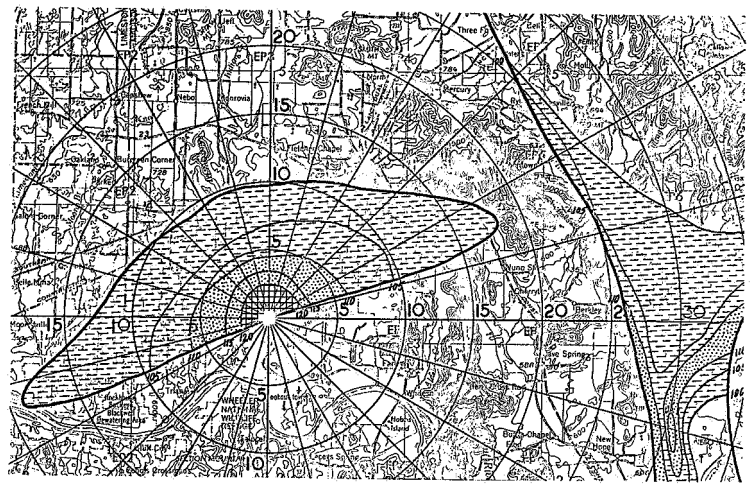

Figure 32

## SOUND INTENSITY LEVELS

RAWINSONDE MEASUREMENT: T-45 MINUTES

(FOR STATIC FIRING: NOV. 23, 1964)

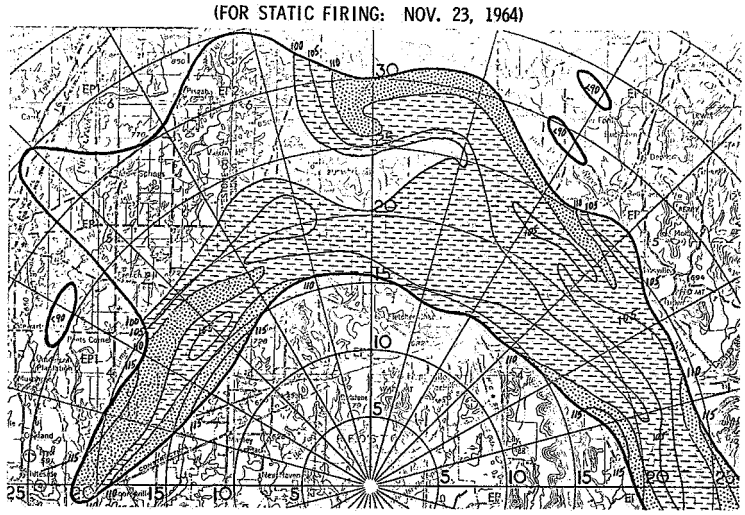

Figure 33

## SOUND INTENSITY LEVELS

RAWINSONDE MEASUREMENT; T-0 MINUTES

(FOR STATIC FIRING: NOV. 23. 1964)

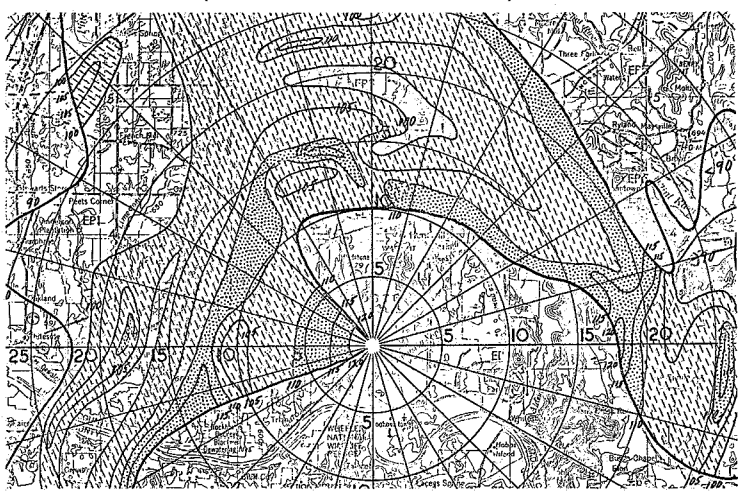

Figure 34

## SOUND INTENSITY LEVELS

RAWINSONDE MEASUREMENT; T+36 MINUTES

(FOR STATIC FIRING: NOV. 23, 1964)

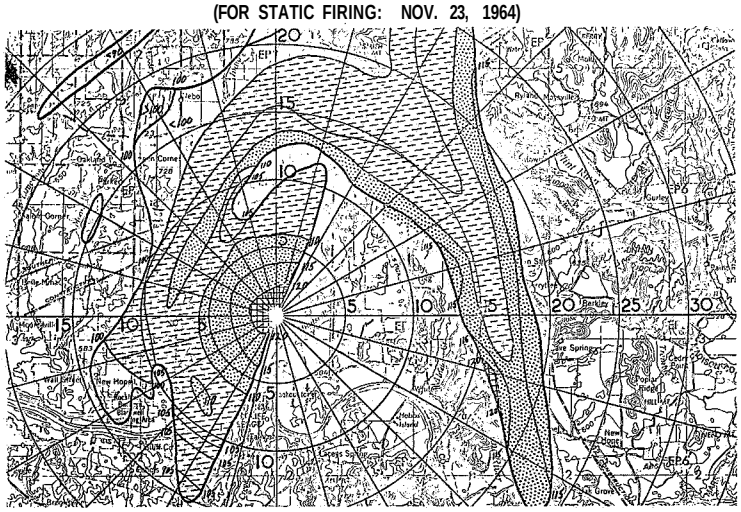

Figure 35

COMPARISON OF SOUND INTENSITY LEVEL AND MEASURED OVERALL SOUND PRESSURE LEVEL FROM ACOUSTICAL HORN FOR CONDITION OF UNIFORM RAYS RETURNING
JANUARY 1963 TO JUNE 1963

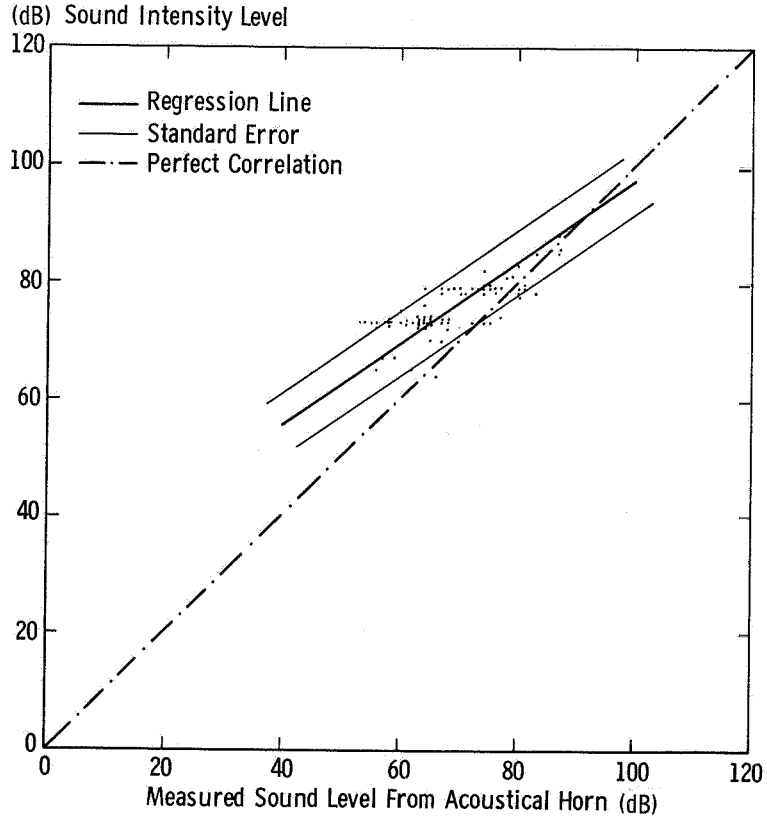


Figure 36

COMPARISON OF SOUND INTENSITY LEVEL FOR ALL CASES (FOCUSING CONDITIONS AND UNIFORM RAYS RETURNING) WITH MEASURED OVERALL SOUND PRESSURE LEVEL FROM ACOUSTICAL HORN
JANUARY 1963 TO JUNE 1963

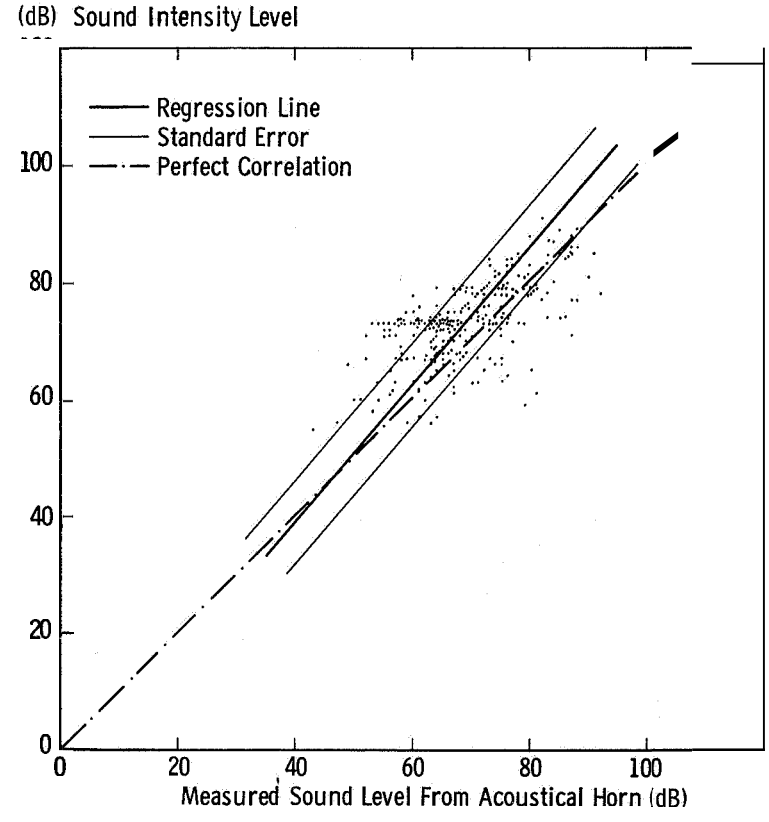


Figure 37

FREQUENCY OF RAYS RETURNING WITH RESPECT TO AZIMUTHS

JANUARY (1962-1963)

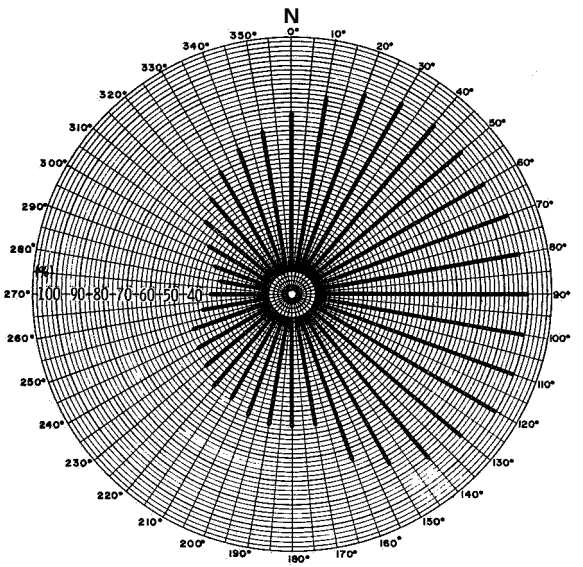


Figure 38

FREQUENCY OF RAYS RETURNING WITH RESPECT TO AZIMUTHS

JULY (1962-1963)

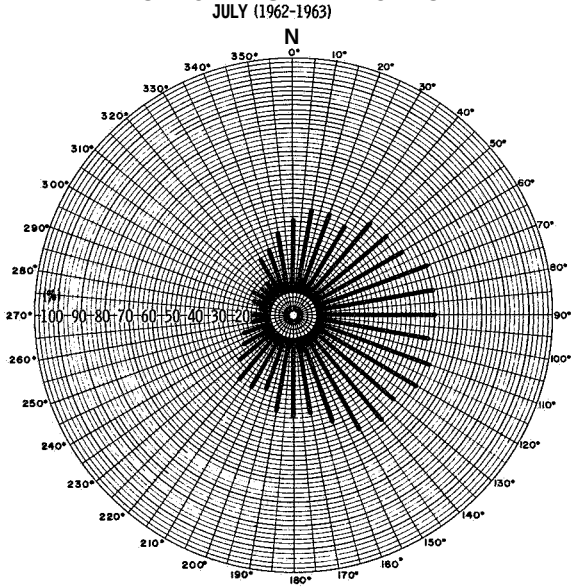


Figure 39

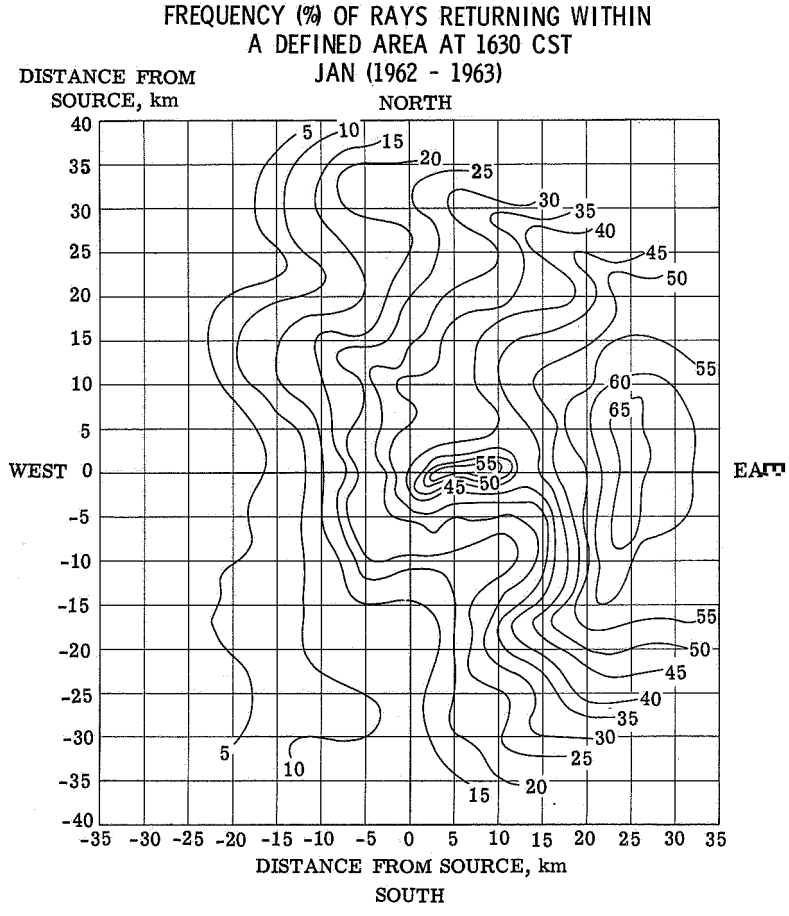


Figure 40

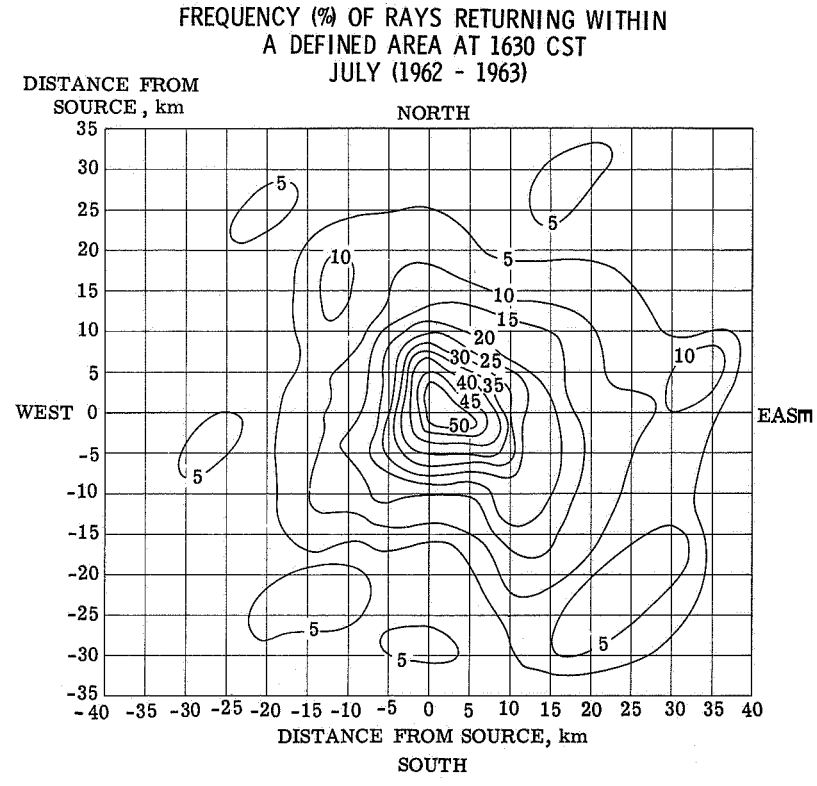


Figure 41

FREQUENCY (%) OF THE RAYS THAT RETURNED AT 1630 CST WHICH PRODUCED SOUND INTENSITY LEVELS $\geq$ 110dB FOR SATURN V

JAN (1962 - 1963)

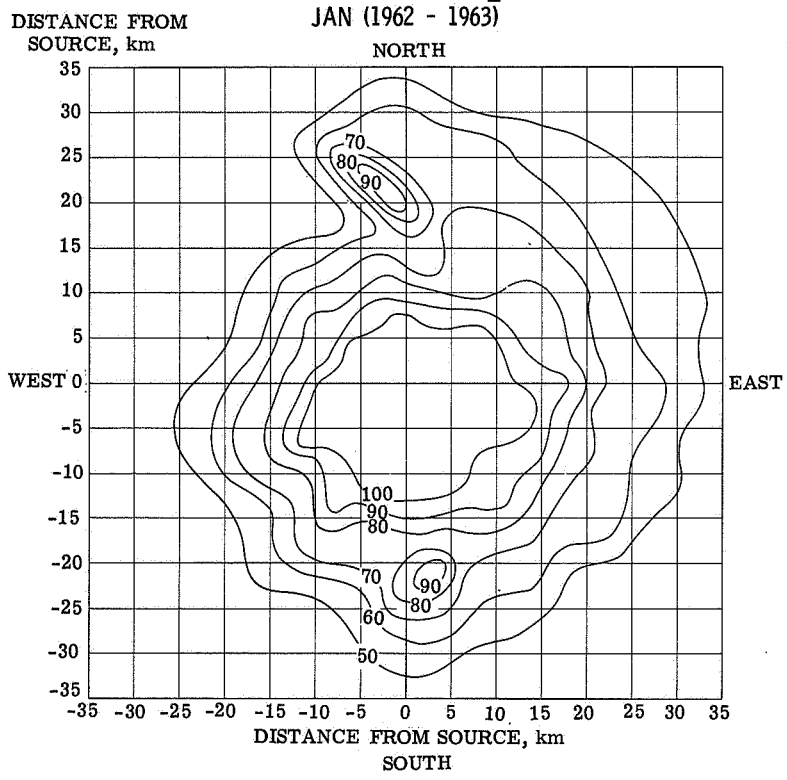


Figure 42

FREQUENCY (%) OF THE RAYS THAT RETURNED AT 1630 CST WHICH PRODUCED SOUND INTENSITY LEVELS $\geq$ 110dB FOR SATURN V

JULY (1962 - 1963)

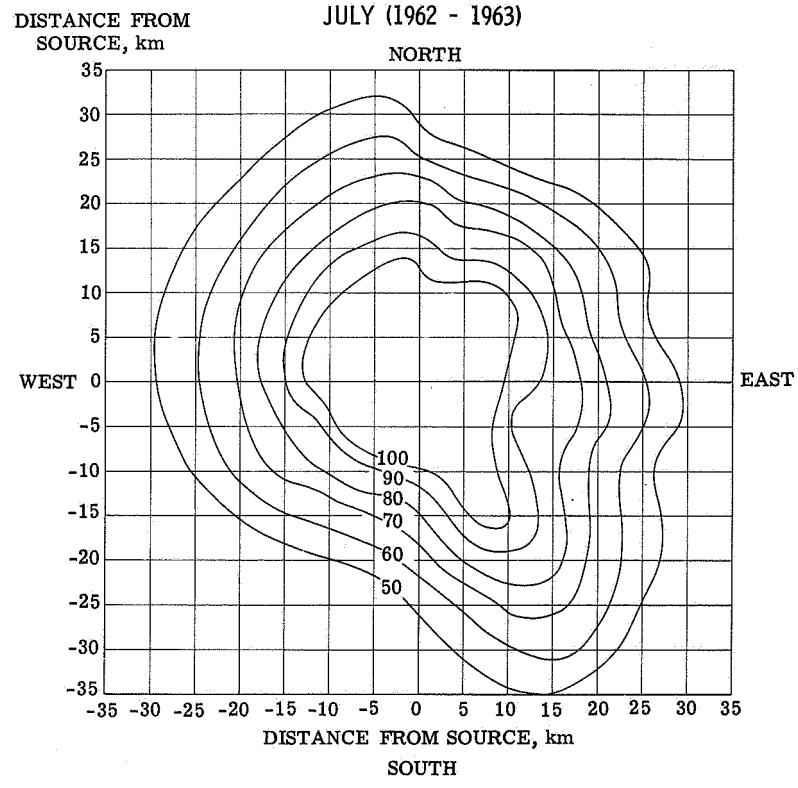


Figure 43